Development of high-affinity nanobodies specific for $Na_V1.4$ and $Na_V1.5$ voltage-gated sodium channel isoforms

Received for publication, January 19, 2022, and in revised form, February 16, 2022 Published, Papers in Press, February 21, 2022,
https://doi.org/10.1016/j.jbc.2022.101763

Lakshmi Srinivasan[1], Vanina Alzogaray[2], Dakshnamurthy Selvakumar[3], Sara Nathan[1], Jesse B. Yoder[1], Katharine M. Wright[1], Sebastián Klinke[2], Justin N. Nwafor[1], María S. Labanda[2], Fernando A. Goldbaum[2], Arne Schön[4], Ernesto Freire[4], Gordon F. Tomaselli[5], L. Mario Amzel[1,†], Manu Ben-Johny[6], and Sandra B. Gabelli[1,5,7,*]

From the [1]Department of Biophysics and Biophysical Chemistry, The Johns Hopkins School of Medicine, Baltimore, Maryland, USA; [2]Fundación Instituto Leloir, IIBBA-CONICET, Buenos Aires, Argentina; [3]ForteBio, Sartorius BioAnalytical Instruments, Fremont, California, USA; [4]Department of Biology, The Johns Hopkins University Krieger School of Arts and Science, Baltimore, Maryland, USA; [5]Department of Medicine, The Johns Hopkins University School of Medicine, Baltimore, Maryland, USA; [6]Department of Physiology and Cellular Biophysics, Columbia University, New York, New York, USA; [7]Department of Oncology, The Johns Hopkins University School of Medicine, Baltimore, Maryland, USA

Edited by Mike Shipston

Voltage-gated sodium channels, Na_Vs, are responsible for the rapid rise of action potentials in excitable tissues. Na_V channel mutations have been implicated in several human genetic diseases, such as hypokalemic periodic paralysis, myotonia, and long-QT and Brugada syndromes. Here, we generated high-affinity anti-Na_V nanobodies (Nbs), Nb17 and Nb82, that recognize the $Na_V1.4$ (skeletal muscle) and $Na_V1.5$ (cardiac muscle) channel isoforms. These Nbs were raised in llama (*Lama glama*) and selected from a phage display library for high affinity to the C-terminal (CT) region of $Na_V1.4$. The Nbs were expressed in *Escherichia coli*, purified, and biophysically characterized. Development of high-affinity Nbs specifically targeting a given human Na_V isoform has been challenging because they usually show undesired cross-reactivity for different Na_V isoforms. Our results show, however, that Nb17 and Nb82 recognize the $CTNa_V1.4$ or $CTNa_V1.5$ over other CTNav isoforms. Kinetic experiments by biolayer interferometry determined that Nb17 and Nb82 bind to the $CTNa_V1.4$ and $CTNa_V1.5$ with high affinity (K_D ~ 40–60 nM). In addition, as proof of concept, we show that Nb82 could detect $Na_V1.4$ and $Na_V1.5$ channels in mammalian cells and tissues by Western blot. Furthermore, human embryonic kidney cells expressing holo $Na_V1.5$ channels demonstrated a robust FRET-binding efficiency for Nb17 and Nb82. Our work lays the foundation for developing Nbs as anti-Na_V reagents to capture Na_Vs from cell lysates and as molecular visualization agents for Na_Vs.

The nine human isoforms of voltage-gated sodium channels ($Na_V1.1$–1.9) rapidly respond to changes in cellular membrane potential by allowing the passage of Na^+ ions into the cell. They play an important role in the generation of the action potential in excitable tissues, such as skeletal muscle, heart, and nerves (1). Mutations in the cytoplasmic C-terminal (CT) region of these proteins have been implicated in human genetic diseases, such as generalized epilepsy with febrile seizures, hypokalemic periodic paralysis, myotonia, long-QT syndrome, and Brugada syndrome (2–4). Given the physiological importance of the Na_V isoforms in normal physiology and disease, development of reagents for their study, such as antibodies (Abs), has been an important part of Na_V research. Specifically targeting each individual isoform, however, has been challenging, because of their high sequence identity. To achieve tissue specificity and avoid off-target side effects of anti-Pan Na_V Abs, there is an increasing need for biologicals with high solubility, stability, and specificity (5, 6).

Nanobodies (Nbs) are single variable heavy-chain (VHH) immunoglobulin domains derived from heavy-chain–only Abs produced in camelids, such as camels, llamas (*Lama glama*), and alpacas. Nbs are small prolate-shaped molecules (~15 kDa) that fully retain the epitope-recognizing function in a single-chain Ab. They may be selected to contain an extended and flexible complementarity-determining region 3 (CDR3) loop partly contributing to their high epitope affinity and their ability to better access smaller and cryptic epitopes (7). Moreover, VHH domains are amenable to cloning and protein modifications and can be produced in bacterial expression systems in scalable amounts. Nbs also display superior solubility, stability, *in vivo* half-lives, and pharmacodynamics compared with conventional Abs (8). For example, Nbs to P2x channel proteins have been shown to display greater therapeutic potential than conventional Abs for modulating channel function and reducing the *in vivo* inflammation caused by P2X7 (9–12). Nbs have also been used as

† This article is dedicated to the memory of Dr L. Mario Amzel.

* For correspondence: Sandra B. Gabelli, gabelli@jhmi.edu.
Present address for Jesse B. Yoder: Hauptman-Woodward Medical Research Institute, Buffalo, NY 14203 USA; Industrial Macromolecular Crystallography Association – Collaborative Access Team (IMCA-CAT), Advanced Photon Source, Argonne National Laboratory, 9700 S. Cass Avenue, Argonne, IL 60439, USA

crystallization chaperones (7, 13, 14), visualization agents (15–17), *in vivo* radiotracers (18), pulldown baits (19, 20), intracellular pathway modulators (21), virus neutralization agents (22, 23), and therapeutics agents (24–27). In this study, we have raised, selected, and characterized Nb clones that recognize the CT region of two Na_V isoforms: $Na_V1.4$ (skeletal muscle) and $Na_V1.5$ (cardiac muscle). We selected the CT domain to serve as an antigen for Nb production since the sequences are more divergent than in other regions of the channels such as the pore-forming regions. Furthermore, the CT domain of the channel is the binding site for channel-interacting proteins, which regulate their activity. This would potentially allow the selection of Nbs that are specific for a given isoform or to a particular state of the channel. Moreover, the available cryo-EM structures have not fully resolved details of these functionally relevant $CTNa_V$ domains. Hence, Nbs targeted to the CT could potentially stabilize these regions, thereby aiding their structure elucidation. In this study, we detail the production, biophysical characterization, and unique structural features of two Nbs that recognize $Na_V1.4$ and $Na_V1.5$ channels and show results highlighting their potential to serve as molecular tools to study Na_V proteins *in vitro* as well as in cells and tissues.

Results

Generation and identification of $Na_V1.4$-specific Nbs

To facilitate the selection of Nbs with isoform specificity, we analyzed the homology amongst Na_V isoforms to choose a divergent region. Sequence homology analysis amongst the Na_V isoforms revealed that the linker between domains 1 and 2 (1–2 linker, amino acids 481–581 in $Na_V1.4$) is the most divergent with pairwise identity between 40 and 55%, whereas the $CTNa_V$ (1599–1836 amino acids in $Na_V1.4$) domain displays pairwise identity of 60 to 70% (Table S1). The fact that $CTNa_V$–calmodulin (CaM) is known to fold as a globular domain that can be purified and crystallized (28, 29) cemented the $CTNa_V$ domain in complex with CaM ($CTNa_V$–CaM) as the antigen of choice. To generate, select, and produce the Nbs (Fig. 1), a llama was immunized with purified $CTNa_V1.4T$ in complex with CaM ($CTNa_V1.4T$–CaM, amino acids 1599–1764 $CTNa_V1.4T$, Table S2 and Fig. 1, step 1 and 2), and its humoral immune response was evaluated by ELISA (Figs. S1*A* and 1, steps 3 and 4) (29). mRNA was extracted from isolated peripheral blood lymphocytes (PBLs; Fig. 1, step 4) and PCR amplified (Fig. 1, step 5). The VHH complementary DNA (cDNA) was cloned into a phagemid vector pHEN4 to obtain the VHH phage library (Fig. 1, step 6).

To identify Nbs that target $CTNa_V1.4$–CaMs, we screened an Nb phage display library with an estimated complexity of $>5.6 \times 10^7$ clones (Fig. 1, step 7). Following two rounds of positive selection against $CTNa_V1.4T$–CaM, a total of 87 randomly chosen clones were expressed and tested by ELISA (Fig. 1, step 8). Amongst them, 14 clones were found specific to $CTNa_V1.4$–CaM (Fig. S1*B*). We further classified the 14 clones into four different families based on the length and variability of their CDR2 and CDR3 regions (Fig. S1*C*). One representative clone from each family was chosen and screened by periplasmic ELISA against $CTNa_V1.4T$–CaM, Ca^{2+} CaM, and apoCaM proteins (Fig. 2*A*). Of these, Nb17, Nb30, and Nb82 were found to be specific to $CTNa_V1.4T$–CaM ("+" signs) but not to Ca^{2+} CaM or apo-CaM. However, Nb26 recognized not only $CTNa_V1.4T$–CaM but also Ca^{2+} CaM and apo-CaM. Based on this information, Nb17, Nb30, and Nb82 were chosen for expression and purification in *Escherichia coli* for further biophysical and biochemical characterization. The three selected Nb clones were subcloned into a pHEN6-His vector as a CT 6×-His tagged fusion protein and successfully expressed in the periplasm of *E. coli* Rosetta-gami 2(DE3) cells. The Nbs were extracted from the periplasm using a combination of thermal and osmotic shock methods (30). Of these, Nb30 was not pursued further because of its low expression levels. Nb17 and Nb82 were purified *via* nickel–nitrilotriacetic acid (Ni–NTA) chromatography, followed by size-exclusion chromatography (SEC; Figs.1, step 9 and 2, *B–D*). Both Nbs behave as monomers in solution and were detected as a single homogenous peak on SEC with retention volumes of 14.4 ml (Nb17) and 15.6 ml (Nb82) on a Superdex 75 10/300 GL column (Fig. 2*D*). These retention volumes are in agreement with those of Nbs reported in the literature (31, 32).

Nb17 and Nb82 are thermally stable

The temperature stability of Nb17 and Nb82 was measured by differential scanning calorimetry (DSC). Nb17 is characterized by a T_m of 76 °C (Fig. 3*A*) and Nb82 by a T_m of 66 °C (Fig. 3*B*), suggesting both are relatively stable protein suitable for functional and structural characterization. Notably, Nb17 undergoes reversible temperature denaturation, whereas Nb82 undergoes irreversible denaturation. The different denaturation mechanisms probably originate from sequence differences. These different mechanisms are also reflected in the shape of the DSC curves (33). Also, Nb17 has a van't Hoff enthalpy of 118 kcal/mol that is close to what is expected for a protein of this size undergoing two-state unfolding. For Nb82, the irreversible transition is kinetically controlled, with a noticeable change in shape of the curve, and characterized by an activation energy of 86 kcal/mol.

Nb82 has an extended CDR3 loop

The structure of Nb82 was determined by X-ray crystallography to 2.0 Å resolution and refined to an R_{work}/R_{free} of 0.19/0.24 with excellent geometry (Protein Data Bank [PDB] ID: 7R63; Table 1 and Fig. 3, *C–F*). The asymmetric unit includes four copies of Nb82 with almost identical conformations (Cα RMSD <0.30 Å, pairwise among all four chains, including 117 Cα carbons). Nb82 bears the classical immunoglobulin fold (Fig. 3, *C* and *D*) with two β-sheets of four antiparallel β-strands (β1–β3–β8–β7 and β6–β5–β4–β9) and a smaller β-sheet made up of two parallel β-strands, β2 and β10, that elongate the β6–β5–β4–β9 sheet. The structure displays good electron density for all portions of the four molecules (Table 1 and Fig. 3, *C* and *D*). The fold is decorated by three π-helices, two of which are in the epitope-recognizing CDR1 and CDR3, formed between the β3–β4 and β9–β10 loops,

respectively. The third π-helix is on the loop connecting strands β3 and β4. CDR π-helices are a characteristic feature observed in other Nbs (14). CDR3, the usual major contributor for antigen recognition and specificity, folds as a random coil with a π-helix of seven residues that folds back onto β6–β5–β4–β9 sheet. Notably, the CDR1 and CDR2 present a positively charged patch (Fig. 3, *E* and *F*) suggesting that Nb82 favors an interaction with a large negatively charged surface on the Na_V. Comparison of the sequence of Nb82 with Nb17 and Nb30 (Fig. 3*G*) and its structure (PDB ID: 7R63) with other Nbs available (PDB IDs: 5LMJ, 6H6Y, and 5LZ0 (14)) (Fig. S2) highlights the differences in the fold of their CDR3 (Fig. S2, *A* and *B*).

Nb17 and Nb82 specifically recognize $CTNa_V1.4$ and $CTNa_V1.5$ isoforms

To evaluate the specificity of the two Nbs, we performed ELISA experiments (Fig. 4*A*) with the purified Nbs and purified $CTNa_V$ isoforms in complex with CaM ($CTNa_V1.4$–CaM, $CTNa_V1.5$–CaM, $CTNa_V1.7$–CaM) and with $CTNa_V1.9$,

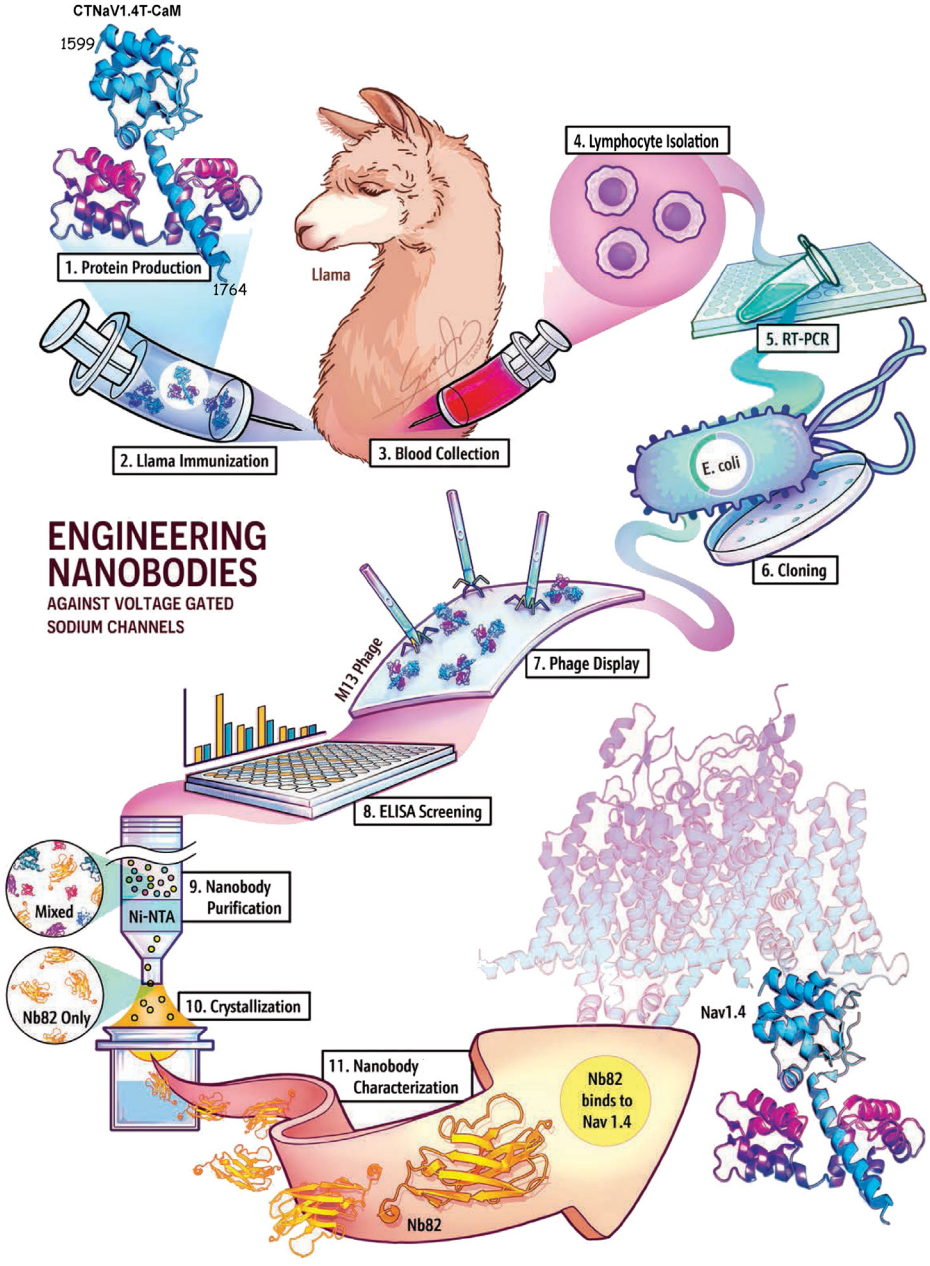

Figure 1. Scheme describing the steps used for the selection of high-affinity nanobodies (Nbs) specific for voltage-gated sodium channels. Step 1: Production of $CTNa_V1.4T$–CaM to use as antigen. Step 2: Llama immunization with $CTNa_V1.4T$–CaM. Step 3: Collection of immune sera from llama on day 35 and day 40 postimmunization. Step 4: Isolation of lymphocytes to extract total RNA. Step 5: RT–PCR to obtain complementary DNA of VHH domains. Step 6: Cloning of VHH complementary DNA (750 bp) into *Escherichia coli* shuttle vector for phage display. Step 7: Phage display for selection of Nbs against $CTNa_V1.4T$–CaM in M13 phage. Step 8: Screening phage library by ELISA for high-binding Nb clones. Step 9: Cloning in pHEN6 vector and purification of selected Nb clones (Nb17, Nb30, and Nb82) in *E. coli*. Step 10: Crystallization of Nb82 using commercially available sparsematrix screens. Step 11: Characterization of Nb binding to $Na_V1.4$ and $Na_V1.5$ isoforms. This rendition was contributed by Sora Ji (Sorajistudio.com). CaM, calmodulin.

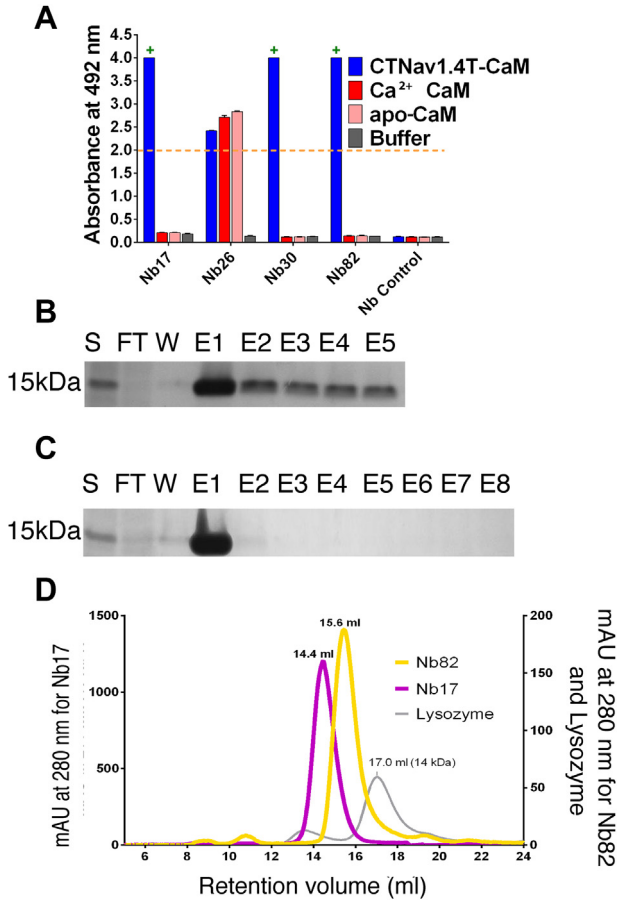

Figure 2. Identification of nanobodies (Nbs) specific for $Na_V1.4$. *A*, ELISA of the periplasmic extract using positively selected clones. Absorbances higher than 2 (*orange dashed line*) were considered positive. "+" signs over Nb17, Nb30, and Nb82 indicate that they are specific to $CTNa_V1.4T$–CaM but not to Ca^{2+} CaM or apo-CaM. *B*, SDS-PAGE gel of IMAC purification of Nb17. *C*, same as (*B*) for Nb82. *D*, size-exclusion chromatogram of Nb17 (17.4 kDa, *purple*) and Nb82 (16.8 kDa, *yellow*). Lysozyme (14 kDa, *gray*) used as gel filtration molecular weight standard is also included. CaM, calmodulin; E, elution fraction; FT, flow-through; IMAC, immobilized metal affinity chromatography; S, supernatant; W, wash.

which does not form a complex with CaM. We used a truncated (T) or full-length (FL) construct of the $CTNa_V$ isoforms (Fig. 4*B*). In ELISA experiments, Nb82 and Nb17 recognize both the T and FL versions of both $CTNa_V1.4$–CaM (skeletal) and $CTNa_V1.5$–CaM (cardiac). However, they do not recognize neuronal isoforms, $CTNa_V1.7$–CaM or $CTNa_V1.9$ (Fig. 4*A*). Importantly, they do not crossreact with free CaM (Fig. 4*A*).

Consistent with these findings, Western blot analysis demonstrated that His-tagged Nb82 as a primary Ab detected purified $CTNa_V1.4T$, $CTNa_V1.4FL$, $CTNa_V1.5T$, and $CTNa_V1.5FL$, resulting in signals corresponding to their respective molecular weights (Fig. 5*A*). On the other hand, no signal was detected for purified $CTNa_V1.7$, $CTNa_V1.9$, CaM alone, and glutathione-*S*-transferase (GST) (Fig. 5*A*), suggesting that Nb82 is specific to $Na_V1.4$ and $Na_V1.5$ channels.

To fully establish the selectivity of Nb17 and Nb82, we utilized a flow cytometry–based FRET two-hybrid assay to systematically probe the interaction of the two Nbs with $CTNa_V1.1$–$CTNa_V1.9$. We engineered Nb17 and Nb82 with a Cerulean fluorescent protein as a FRET donor and the CT domains of $Na_V1.x$ with the Venus fluorescent protein, as FRET acceptor. Stochastic expression of the FRET pairs resulted in variable FRET efficiencies (E_A) in individual cells. A saturating binding relation was then constructed by correlating E_A with the free donor concentration (D_{free}). Nb82 and Nb17 exhibited robust FRET with $CTNa_V1.4$ and $CTNa_V1.5$, whereas other isoforms showed qualitatively weaker FRET (Fig. 5, *B* and *D*). To quantify further, we calculated a relative association constant, $K_{a,EFF}$ (in arbitrary units) as $1/K_{d,EFF}$ (the relative dissociation constant) from the fits in panels *B* and *D*. Indeed, both Nb17 and Nb82 demonstrated 7-fold to 100-fold higher $K_{a,EFF}$ for $Na_V1.4$ and $Na_V1.5$ as compared with other Na_V isoforms (Fig. 5, *C* and *E*). Taken together, these results highlight the exquisite selectivity of Nb17 and Nb82 for the muscle Na_V channels.

Thus affirmed, we further characterized the $CTNa_V$–CaM and Nb82 interactions by analyzing the $CTNa_VX$–CaM + Nb mixtures (where X equals 1.4 or 1.5) by SEC (Fig. 6). In the profiles, we observed that the $CTNa_V1.4T$–CaM + Nb82 (Fig. 6, *A* and *B*) and $CTNa_V1.4FL$–CaM + Nb82 complexes (Fig. 6, *C* and *D*) elute about 2 ml earlier than the equivalent complexes in the absence of Nb82. SDS-PAGE gels of the elution fractions show that the new peaks contain all three proteins; $CTNa_V1.4$, CaM, and the Nb82 (Fig. 6, *B* and *D*). Also, the complexes elute at retention volumes that correspond to the molecular weight of the $CTNa_V1.4$–CaM + Nb complex 1:1 stoichiometry. $CTNa_V1.5$ showed a similar behavior. The complexes $CTNa_V1.5T$–CaM + Nb82 and $CTNa_V1.5FL$–CaM + Nb82 elute 1.0 and 1.5 ml before the $CTNa_V1.5T$–CaM complex, respectively (Fig. 6, *E* and *G*). The SDS-PAGE gels of the peak fractions confirm the presence of all three proteins ($CTNa_V1.5$, CaM, and Nb) (Fig. 6, *F* and *H*).

The mixture of $CTNa_V1.5$–CaM + Nb17 on SEC does not show a fully resolved new peak, typical of the formation of a complex. However, in the $CTNa_V1.5T$–CaM + Nb17 (Fig. S3, *A* and *B*) and $CTNa_V1.5FL$–CaM + Nb17 (Fig. S3, *C* and *D*), peaks elute 0.5 ml before the $CTNa_V$–CaMs without the Nb followed by an asymmetric Nb17 peak. Also, in the SDS-PAGE gels of the elution fractions, the peaks corresponding to the CT $Na_V1.5$–CaM + Nb17 complex shows the presence of all three proteins; $CTNa_V1.5$, CaM, and Nb17. These results imply that both Nb17 and Nb82 interact with the $CTNa_V$–CaMs but affect their hydrodynamic radii differently.

Nbs bind with nanomolar affinities to $Na_V1.4$ and $Na_V1.5$

We further probed the molecular interactions of the $CTNa_V1.4$–CaM + Nb and $CTNa_V1.5$–CaM + Nb ([$CTNa_VX$]–CaM + Nb; X = 1.4 or 1.5) complexes by determining the kinetic parameters of binding using biolayer interferometry (BLI) (Figs. 7 and 8). The change in resonance with time was recorded at different concentrations of purified $CTNa_V1.XT$–CaM proteins or isolated CaM. A 1:1 binding of the Nbs to $CTNa_VXT$–CaM proteins was observed with signals reaching steady state in 300 s. Analysis of the BLI dose responses of association and dissociation curves indicates that Nb82 binds to $CTNa_V1.4T$–CaM and $CTNa_V1.5T$–CaM with

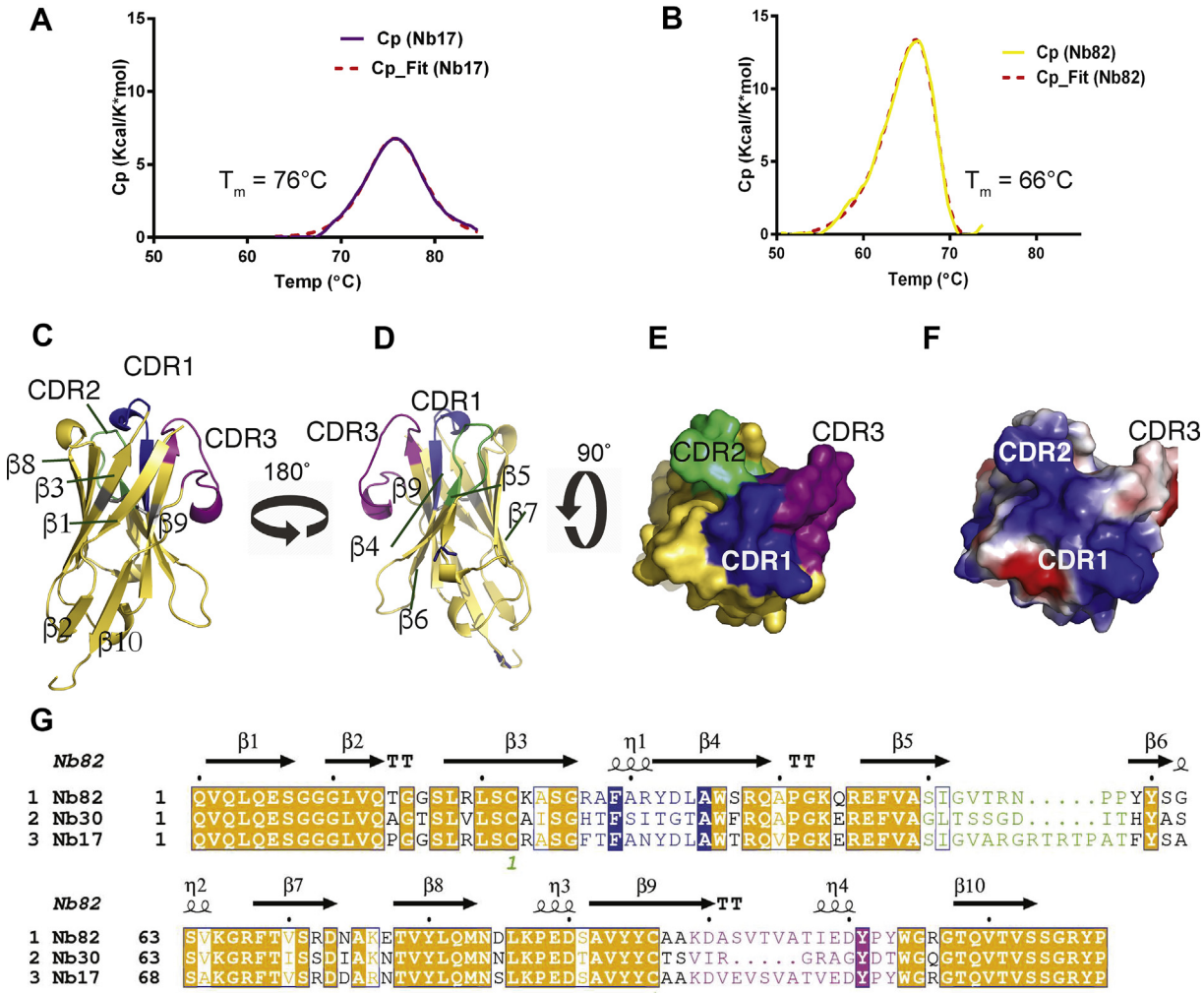

Figure 3. Nanobody (Nb) thermal stability and crystal structure of Nb82. *A*, DSC curve showing the temperature denaturation of Nb17 undergoing reversible denaturation with T_m centered at 75.8 °C. *B*, same as *A*. Nb82 undergoes irreversible denaturation with T_m centered at 66.0 °C. *C*, cartoon representation of Nb82 (*yellow*) displaying the CDR1 (*blue*), CDR2 (*green*), and CDR3 (*magenta*). *D*, same as (*A*) with 180° rotation along the vertical axis. *E*, bird's eye view of Nb82 in (*A*) with surface coloring according to the CDRs. *F*, same as (*C*) with Nb82 surface colored according to the electrostatic charges. *G*, sequence alignment of Nb82, Nb30, and Nb17. The three CDR regions are color coded as CDR1 (*blue*), CDR2 (*green*), and CDR3 (*magenta*). The secondary structure elements of Nb82 are placed on top of the alignment. CDR, complementarity-determining region; DSC, differential scanning calorimetry.

affinities of 50.2 ± 0.1 and 63.2 ± 0.07 nM, respectively (Fig. 7, *A* and *B* and Table 2). However, no binding to Nb82 was observed when isolated CaM was used as an analyte (Fig. 7*C*) evidenced by a nonassociation/no-binding curve. In addition, as estimated from ELISA results, no binding to Nb82 was observed when $CTNa_V1.7T$–CaM or $CTNa_V1.9T$ were used as analytes (Fig. 7, *D* and *E*). Similarly, with Nb17 (Fig. 8, *A* and *B*), BLI experiments show that it binds to $CTNa_V1.4T$–CaM and $CTNa_V1.5T$–CaM with dissociation constants (K_Ds) of 41.0 ± 0.1 nM and 60.5 ± 0.06 nM, respectively (Table 2 and Fig. 8*C*) but not to isolated CaM. Moreover, as expected, no binding to Nb17 was observed when $CTNa_V1.7T$–CaM or $CTNa_V1.9T$ was used as analytes (Fig. 8, *D* and *E*). In these experiments, the lack of binding of Nb17 and Nb82 to isolated CaM and to $CTNa_V1.7$–CaM and $CTNa_V1.9$ indicates that the epitope for Nb82 binding is on the $Na_V1.4(5)$ channels or on the $Na_V1.4(5)$–CaM interface in an area different enough from that of Na_V17 or $Na_V1.9$.

Nb17 and Nb82 detect $Na_V1.5$ channel in live cells and tissue homogenates

To determine whether Nb17 and Nb82 interact with holo-$Na_V1.5$ channels in live cells, we utilized flow cytometry–based FRET two-hybrid assay (34). To do so, we utilized Cerulean-tagged Nb17 and Nb82 as FRET donor, and we attached a Venus tag to the carboxy terminus of the FL $Na_V1.5$ (FRET acceptor) (Fig. 9*A*) and obtained fluorescence measurements using a flow cytometer. Stochastic expression of the FRET pairs resulted in variable FRET efficiencies (E_A) in individual cells. A saturating binding relation was then constructed by correlating E_A with the free donor concentration (D_{free}). We observed robust FRET for both Nb17 (Fig. 9*B*) and Nb82 (Fig. 9*C*) with $Na_V1.5$ confirming baseline association of the heterologously expressed Nb in live cells. By contrast, coexpression of Cerulean alone with $Na_V1.5$ did not show appreciable FRET (Fig. 9*D*). These findings demonstrate the robust interaction of Nb17 and Nb82 with $Na_V1.5$ in live cells, thus

Table 1
Data collection and refinement statistics

Data collection	Nb82 (PDB: 7R63)
Space group	C2221
Cell dimensions	
a, *b*, *c* (Å)	77.7, 82.4, 170.7
α, *β*, *γ* (°)	90.00, 90.00, 90.00
Resolution (Å)[a]	29.67–2.0 (2.052–2.0)
R_{merge}	0.07 (0.39)
R_{pim}	0.030 (0.164)
CC1/2	0.999 (0.985)
⟨I/σ(I)⟩	14.5 (4.2)
Completeness (%)	99.9 (99.9)
Total reflections	249,354 (2845)
Unique reflections	37,476 (473)
Refinement	
R_{work}/R_{free}	0.19/0.24 (0.22/0.28)
No. of atoms	
Protein	4331
Ligand/ion	—
Water	278
B-factors (Å^2)	
Protein	36.0
Water	44.6
RMSD	
Bond lengths (Å)	0.01
Bond angles (°)	1.57
Ramachandran plot	
Favored (%)	97.8
Allowed (%)	1.5
Disallowed (%)	0.7

[a] Values for the outer shell are given in parentheses.

furnishing a new avenue to probe and manipulate Na_V channels in physiology.

Nb82 as a $Na_V1.4$ and $Na_V1.5$ molecular detection reagent

To take advantage of the high affinity of the Nbs for $CTNa_V1.4$ and $CTNa_V1.5$, we used Nb82 as a molecular reagent to detect Na_Vs in cell and tissue lysates by Western blot. His-tagged Nb82 detects $Na_V1.4$ in mouse skeletal muscle homogenates in addition to $Na_V1.5$ in mouse heart homogenates as shown by a band at ∼220 kDa. Notably, Nb82 does not detect Na_Vs in brain tissue (Fig. 9*E*). The Western blot signal detected by the His-tagged Nb82 (Fig. 9*E*) is comparable to that detected by a commercially available anti-Pan Na_V Ab (Fig. 9*F*) as observed by signals corresponding to the same molecular weight for skeletal muscle and heart tissue samples in both blots. Moreover, the anti-Pan Na_v Ab detects a band at ∼250 kDa in mouse brain tissue (Fig. 9*F*) that is not observed with the Nb82 detection. Also, Nb82 detects Nav1.5 from human induced pluripotent stem cell–derived cardiomyocytes (hiPSC–CMs) differentiated from normal hiPSCs as observed by a band at ∼220 kDa (Fig. 9*H*). As a control, when the blots were reprobed with simply anti-His horseradish peroxidase (HRP) Ab (Fig. 9,*G* and *I*), no bands were observed at 220 to 250 kDa showing the specificity of detection by Nb82 as expected.

Discussion

This study describes the generation and characterization of two Nbs, Nb17 and Nb82, that recognize and bind to the voltage-gated sodium channel $Na_V1.4$ and $Na_V1.5$ isoforms. The Nbs do not recognize isolated CaM, $Na_V1.7$, or $Na_V1.9$ channels showing their specificity for the Na_V muscle isoform, $Na_V1.4(5)$. Both Nbs have structural stabilities similar to those observed for other globular proteins. According to the survey of Robertson and Murphy (35), the average T_m for globular proteins is approximately 68 °C compared with the T_ms of 76 and 66 °C for Nb17 and Nb82, respectively. Also, according to the survey of Robertson and Murphy, the mean enthalpy for a protein of 15 kDa at 70 °C is 115 kcal/mol, which is close to the van't Hoff enthalpy of Nb17 suggesting structuring interactions similar to those observed for other proteins. The denaturation transition of Nb82 is irreversible at pH 8.0, which is not unseen for other proteins (36) that nevertheless undergo reversible denaturation at lower pH values.

The crystal structure of Nb82 reveals a long (15 amino acids) CDR3 for a llama-derived Nb that could possibly underlie the nanomolar binding affinities observed for the Nbs to $Na_V1.4$ and $Na_V1.5$.

Nb82 promises to be a high-affinity $Na_V1.4(5)$ protein detection reagent. Our SEC experiments demonstrate formation of stable $CTNa_V1.4(5)$–CaM + Nb complexes. Importantly, binding kinetic experiments by BLI show nanomolar binding affinities for the Nbs to $CTNa_V1.4$–CaM and $CTNa_V1.5$–CaM proteins and no binding to CaM or $CTNa_V1.7$–CaM and $CTNa_V1.9$ proteins. Furthermore, flow-cytometric FRET measurements in human embryonic kidney 293 (HEK293) cells expressing FL $Na_V1.5$ channel display high efficiency of binding of Nb17 and Nb82 to $Na_V1.5$ channels on the cell surface but no binding to CaM-expressing cells. In HEK293 cells expressing $CTNa_V1.4$ or $CTNa_V1.5$ isoforms, flow-cytometric FRET measurements show binding to Nb17 or Nb82. In contrast, cells expressing any of the other $CTNa_V1.x$ isoforms displayed negligible binding. We further demonstrate that Nb82 can be used as a molecular reagent to detect $Na_V1.4(5)$ proteins in various types of cell and tissue lysates since it recognizes endogenous $Na_V1.4$ channel from mammalian skeletal muscle in addition to $Na_V1.5$ from mammalian heart and hiPSC–CMs.

Nbs have been selected for other voltage-gated channel–related subunits. For instance, the auxillary subunit of Ca_V channel, $Ca_v\beta$, has been targeted to design a potent genetically encoded high-voltage–activated calcium channel inhibitor (37). It is worth highlighting that the anti-$Na_V1.4$ and anti-$Na_V1.5$ Nbs produced as part of this study carry a simple CT 6×Histidine tag, ensuring ease of production and scale up of anti-Na_V Nbs to serve as Na_V detection reagents, crystallization chaperones, and as *in vitro* and *in vivo* research tools and molecular probes.

Experimental procedures

Methods

CT $Na_V1.4$–CaM protein expression for llama immunization

The GST-tagged CT region of $Na_V1.4$ (amino acids 1599–1764), in complex with CaM ($CTNa_V1.4T$–CaM), was expressed and purified from BL21-CodonPlus RIL *E. coli* cells using a GST-sepharose. Reduced L-glutathione eluted fractions were proteolyzed with PreScission protease followed by anion exchange chromatography and a final gel filtration chromatography as described by Yoder *et al.* (29). Purified

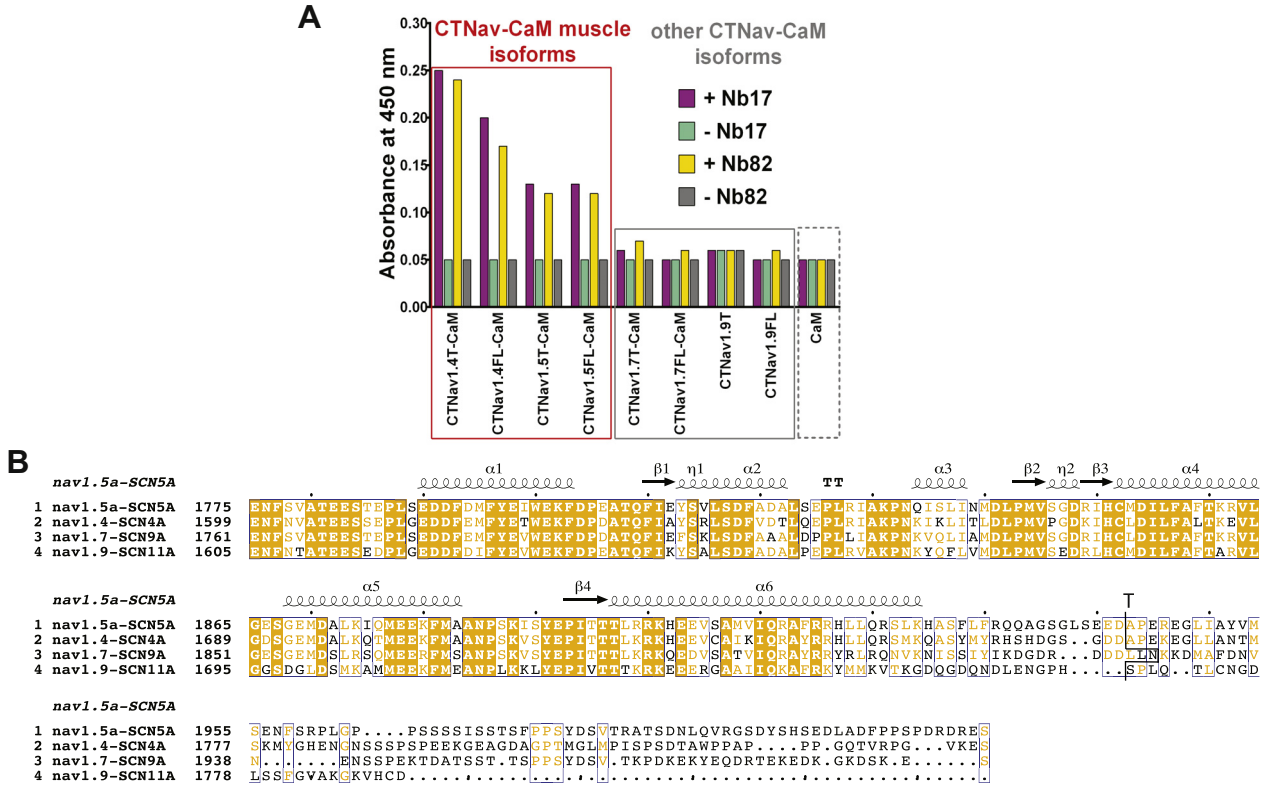

Figure 4. Nb17 and Nb82 recognize the Na_V-muscle isoforms. *A*, ELISA bar graphs using purified Nb17 (*magenta*), the absence of Nb17 (*green*), Nb82 (*orange–yellow*), and the absence of Nb82 (*gray*). The *red box* clusters Na_V proteins that represent muscle isoforms $CTNa_V1.4T$–CaM, $CTNa_V1.4FL$–CaM, $CTNa_V1.5T$–CaM, and $CTNa_V1.5FL$–CaM. The *gray box* clusters the other Na_V isoforms tested, $CTNa_V1.7T$–CaM, $CTNa_V1.7FL$–CaM, $CTNa_V1.9T$, $CTNa_V1.9FL$, and CaM. Data are representative of three independent experiments. *B*, sequence alignment of $CTNa_V1.4FL$, $CTNa_V1.5FL$, $CTNa_V1.7FL$, and $CTNa_V1.9FL$ proteins. The *black trace* indicates the limits of the T $CTNa_VT$–CaM constructs. CaM, calmodulin; FL, full length; Nb, nanobody; T, truncated.

$CTNa_V1.4T$–CaM at 56 mg/ml was used for generation of single-chain Abs by llama immunization.

Llama immunization and construction of Nb library

The immunization protocol and the construction of the library were done as previously described (30, 38). In brief, llama was immunized three times intramuscularly every 15 days with 100 μg of purified $CTNa_V1.4T$–CaM emulsified with complete Freund's adjuvant. The humoral immune response in the sera was monitored by ELISA performed in plates coated with $CTNa_V1.4T$–CaM. Forty-five days after the first immunization (D45), the animal was bled. PBLs were isolated from 300 ml of blood by Ficoll–Paque gradient centrifugation. Total RNA was purified from these cells and subjected to cDNA synthesis. The Nb coding regions were amplified by PCR using specific primers: forward (fwd_001): 5′-GTCCTGGCTGCTCTT CTACAAGG-3′; reverse (rvd_002): 5′-GGTACGTGCTGTT-GAACTGTTCC-3′. The amplicons were purified from agarose gels, digested with PstI and NotI, and cloned into the pHEN4 phagemid vector downstream of the PelB-leader peptide and upstream of the hemagglutinin (HA) tag. *E. coli* TG1 cells were transformed with this vector for obtaining a phage display library. About 15 clones randomly chosen from the library were used for plasmid DNA preparation and run on agarose gel electrophoresis for qualitative analysis, where ˃70% of clones were found to be positive for Nbs.

Phage display selection of $Na_V1.4$–CaM-specific Nbs

The panning was performed in MaxiSorp plates. Briefly, wells were sensitized with either 1 μg of $CTNa_V1.4T$–CaM + 1 mM DTT or uncoated to serve as negative controls. After blocking with 3% skimmed milk in PBS, 1×10^{12} phages in PBS were added to each test and control coated wells and incubated for 2 h at room temperature (RT). Wells were then extensively washed with 25 mM Tris, 150 mM NaCl, 1 mM DTT, 0.05% Tween-20, pH 8.0, and bound phages were eluted with 0.25 mg/ml trypsin. Eluted phages were titrated and subjected to rounds of panning following the same procedure. Output phage titers were estimated by infection of TG1 cells and plating them on LB with 100 μg/ml ampicillin and 2% glucose. A total of 87 randomly chosen clones were grown in deep-well plates containing 1 ml of 2× TY (Tryptone 16 g, yeast extract 10 g, NaCl 5 g per L) medium added with 100 μg/ml ampicillin and 0.1% glucose for 3 h at 37 °C and 200 rpm until cell growth reached the exponential phase. The expression of Nbs was induced by adding 1 mM IPTG per well with shaking at 200 rpm for 4 h at 28 °C. The Nbs were obtained from the periplasm and tested by ELISA on plates sensitized with 1 μg of $CTNa_V1.4T$–CaM. After washing with 25 mM Tris, 150 mM NaCl, 1 mM DTT, 0.05% Tween-20, pH 8.0, Nbs were detected by incubation with anti-HA Ab and developed using antirat IgG peroxidase conjugate. About 14 positive clones were selected for sequencing using universal M13

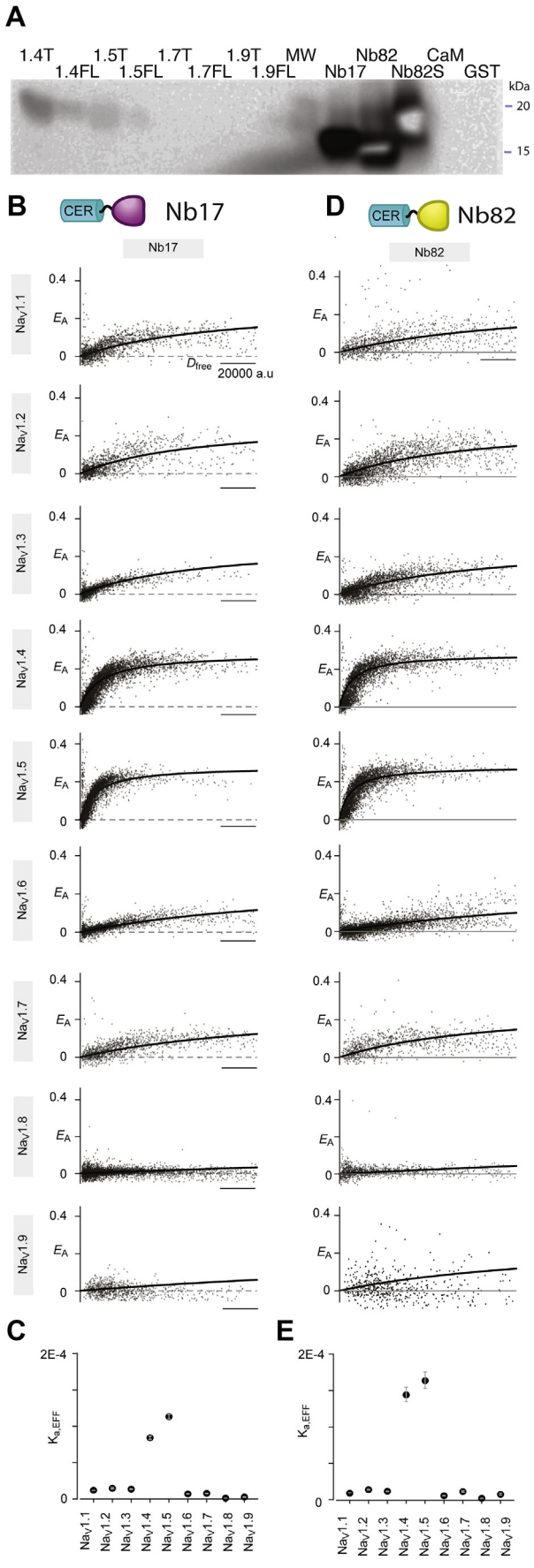

reverse as primer and then classified in families based on the length and variability of their CDR2 and CDR3. Multiple sequence alignments were done with Clustal Omega (39). One representative clone for each family was selected for periplasmic Nb expression, purification, and further characterization. To determine whether the clones from the four families of Nbs recognize $CTNa_V1.4$–CaM or apo CaM, periplasmic-extract ELISA was performed. MaxiSorp plates were sensitized with 0.1 μg of either $CTNa_V1.4T$–CaM, Ca^{2+} CaM, or apoCaM for 2 h at RT and then blocked with 5% bovine serum albumin (BSA) for 2 h at RT. After removal of blocking solution, 50 μl of a 1:100 dilution of TG1 periplasmic extracts expressing each Nb (Nb17, Nb26, Nb30, and Nb82) were incubated overnight at 4 °C (30). Nbs were detected using anti-HA-tag high-affinity secondary Ab by ELISA developed using an antirat IgG peroxidase–conjugated Ab. Nb17, Nb30, and Nb82 were then subcloned in pHEN6 vector. The coding regions were amplified by PCR using the following specific primers: forward (A6E): 5′-GATGTGCAGCTGCAGGAGTCTGGRGGAGG-3';reverse (p38): 5′-GGACTAGTGCGGCCGCTGGAGACGGTGACCTGGGT-3'. The amplicons were purified from agarose gels, digested with restriction enzymes PsTI and BstEII, and cloned into the pHEN6-TEV-His vector for periplasmic expression of recombinant Nbs in *E. coli* Rosetta-gami 2 (DE3) cells. Nb82-His cloned into pHEN6-TEV-His was subcloned to generate Nb82-His-StrepII.

Purification of Nbs Nb17 and Nb82

The expression and purification of the Nbs was performed as described previously with minor modifications (30). Transformed *E. coli* Rosetta-gami 2 (DE3) cells were grown in LB medium supplemented with 100 μg/ml of carbenicillin, 50 μg/ml of kanamycin, and 20 μg/ml of chloramphenicol in addition to 1 mM $MgCl_2$ and 0.1% glucose. Proteins were expressed by inducing the cultures with 1 mM IPTG at an absorbance of 0.8 to 0.9 at 600 nm at 18 °C at 200 rpm overnight. Cells were harvested by centrifugation and frozen at −80 °C for at least 2 h before proceeding to thawing and

Figure 5. Selectivity of Nb17 and Nb82 in detecting $Na_V1.4$ and $Na_V1.5$ channels. *A*, Western blot of purified $CTNa_V$–CaM proteins, CaM alone, and Nb17-His, Nb82-His, CaM, and GST alone showing positive signals for $CTNa_V1.4T/FL$ (1.4T/1.4FL), $CTNa_V1.5T/FL$ (1.5T/1.5FL), and Nb17, Nb82-His and Nb82-StrepII (Nb82S). No signal is observed in the lanes that contained $CTNa_V1.7T/FL$ and $CTNa_V1.9T/FL$ suggesting that Nb82 does not recognize these two isoforms. Western blot was developed using Nb82-His as primary antibody and anti-HisHRP antibody as secondary. All Western blot data show one representative experiment of three. $CTNa_V$–CaM proteins are labeled $CTNa_V1.xT$ (1.xT) and $CTNa_V1.xFL$ (1.xFL). *B*, Nbs tethered to Cerulean serve as a FRET donor, whereas Venus attached to amino-terminal region of $CTNa_V1.x$ serves as a FRET acceptor. Robust FRET is observed between Nb17 and $CTNa_V1.4/5$. Other $CTNa_V$s demonstrate reduced binding. FRET efficiency (E_A) is plotted against the free donor concentration (D_{free}). Each cell represents data from a single cell. *C*, the relative association constant, $K_{a,EFF}$ (in arbitrary units) computed as 1/Kdeff from the fits in (*A*), demonstrates the preference of Nb17 for $CTNa_V1.4/1.5$ over other Na_V isoforms. *D*, analysis of Nb82 shows strong FRET with $CTNa_V1.4/5$. Other Venus-$CTNa_V1.x$ isoforms exhibit weaker binding. *E*, the $K_{a,EFF}$ values confirm strong preference of Nb82 for $CTNa_V1.4/5$ over other $CTNa_V1.x$ isoforms. CaM, calmodulin; FL, full length; GST, glutathione-*S*-transferase; HRP, horseradish peroxidase; Nb, nanobody; T, truncated.

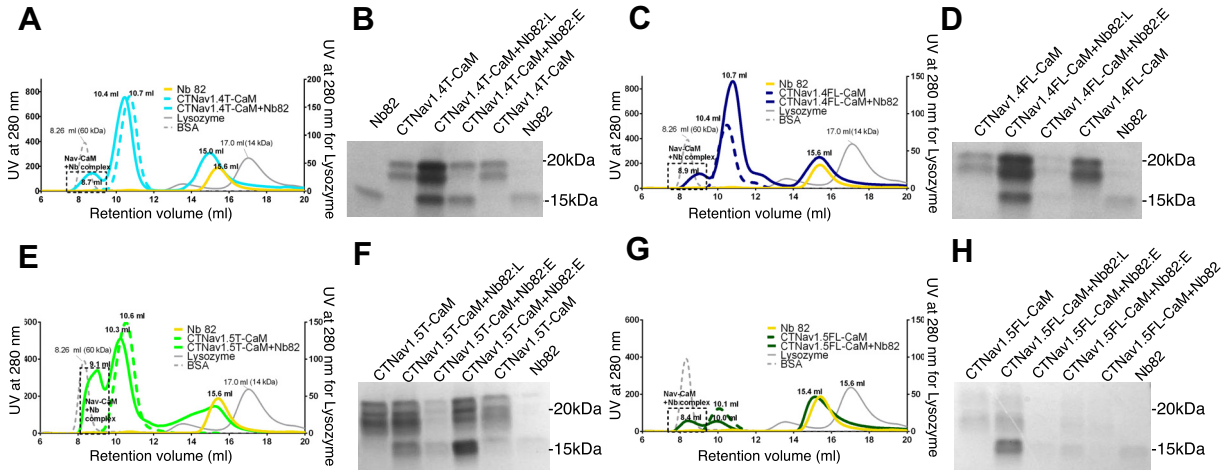

Figure 6. Nb82 forms a complex with $CTNa_V1.4$–CaM and $CTNa_V1.5$–CaM detected by size-exclusion chromatography (SEC). *A*, SEC profile for $CTNa_V1.4T$–CaM + Nb82 (*solid blue line*) showing the appearance a new peak to the left of the $CTNa_V1.4T$–CaM peak (*dashed line*) indicating complex formation. *B*, SDS-PAGE gel showing elution fractions from (*A*). The $CTNa_V1.4T$–CaM + Nb82 complex elutes at 8.7 ml. *C* and *D*, same as *A* and *B*, using construct $CTNa_V1.4FL$–CaM. The $CTNa_V1.4FL$–CaM + Nb82 elutes at 8.9 ml. *E*, SEC profile for $CTNa_V1.5T$–CaM + Nb82 (*solid green line*) showing the appearance of the peak of the complex to the left at 9.1 ml compared with $CTNa_V1.5T$–CaM (*dashed line*) at 10.6 ml. *F*, SDS-PAGE gel showing elution fractions from (*E*). *G* and *H*, same as (*E*) and (*F*) using construct $CTNa_V1.5FL$–CaM. The $CTNa_V1.5FL$–CaM + Nb82 complex elutes at 8.4 ml. Gel filtration molecular weight standards. BSA (66 kDa, *dashed gray line*) and lysozyme (14 kDa, *solid gray line*) are included in *A*, *C*, *E*, and *G*. BSA, bovine serum albumin; CaM, calmodulin; FL, full length; Nb, nanobody; T, truncated.

osmotic shock to extract the periplasmic proteins. For this, cells were thawed in a water bath, resuspended in osmotic-shock TES (0.2 M Tris–HCl, 0.65 mM EDTA, and 0.5 M sucrose, pH 8.0) buffer, and incubated at 4 °C for 1 h on an orbital shaker. Then, cells were further diluted with osmotic-shock TES buffer and incubated at 4 °C for 45 min on an orbital shaker. The periplasmic fraction was isolated by centrifugation at 8000 rpm at 4 °C for 30 min using an SLA1500 rotor. To the filtered supernatant (0.22 μm polyethersulfone filter), 2.5 mM Tris(2-carboxyethyl)phosphine and 5 mM imidazole were added and incubated overnight with 1 ml of prewashed Ni–NTA agarose Superflow beads at 4 °C using an orbital shaker. The Ni–NTA agarose beads were equilibrated with 50 mM Tris, 150 mM NaCl, pH 8.0

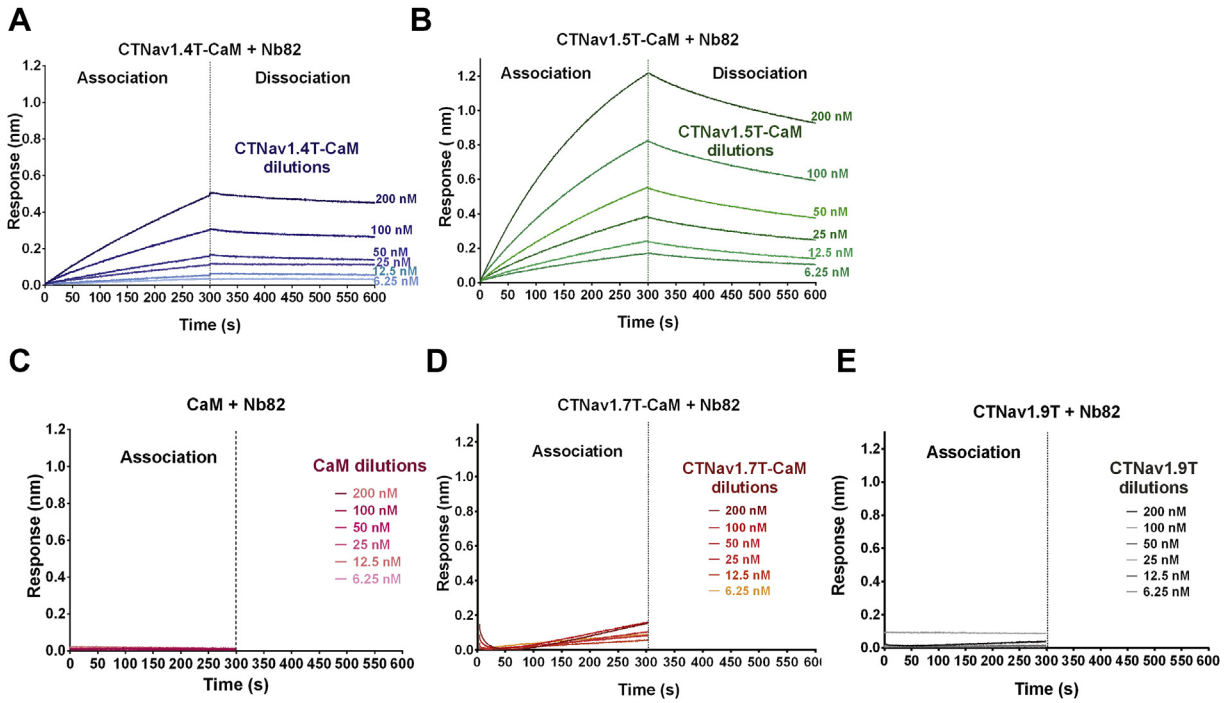

Figure 7. Nb82 binds to $CTNa_V1.4T$–CaM and $CTNa_V1.5T$–CaM with nanomolar affinity. *A*, BLI sensorgram of Nb82 titrated with $CTNa_V1.4T$–CaM at concentrations 6.25, 12.5, 25, 50, 100, and 200 nM plotted as nanometer shift with time. *B*, same sensorgram as *A* but for Nb82 titrated with $CTNa_V1.5T$–CaM. *C*–*E*, sensorgrams showing no binding of Nb82 to CaM alone, $CTNa_V1.7T$–CaM, or $CTNa_V1.9T$, respectively. BLI, biolayer interferometry; CaM, calmodulin; Nb, nanobody; T, truncated.

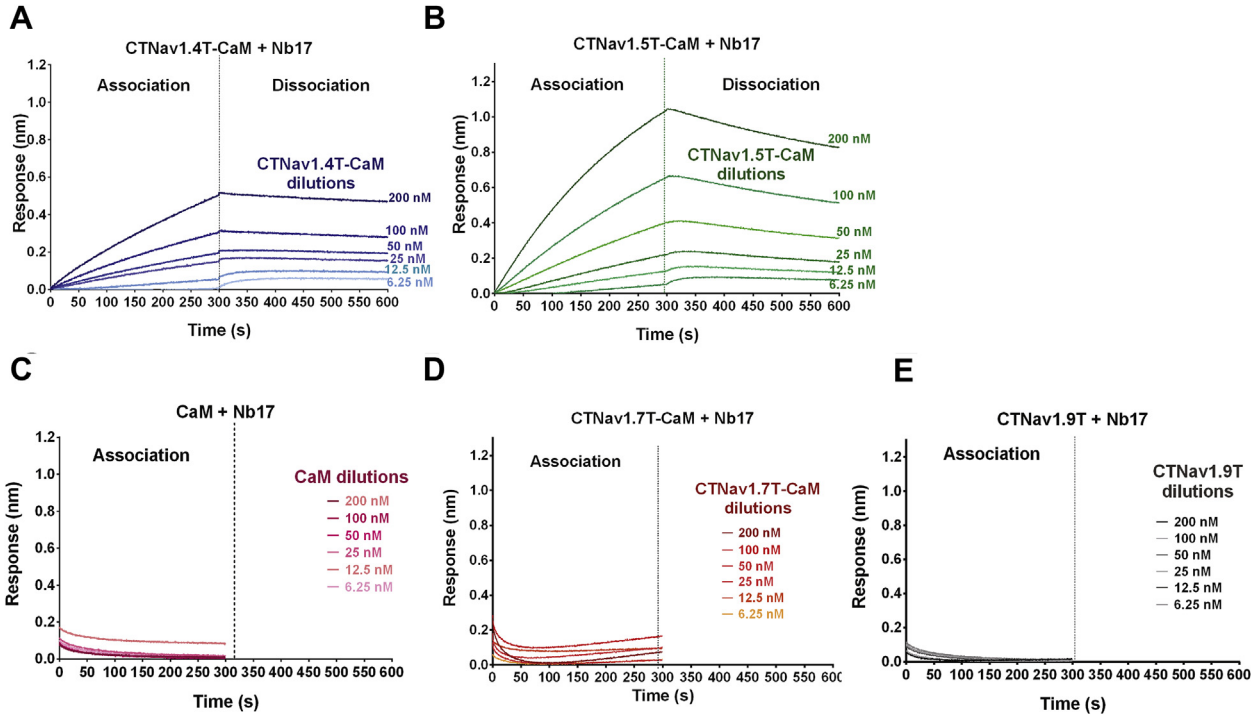

Figure 8. Nb17 binds to $CTNa_V1.4T$–CaM and $CTNa_V1.5T$–CaM with nanomolar affinity. *A*, BLI sensorgram of Nb17 titrated with $CTNa_V1.4T$–CaM at concentrations 6.25, 12.5, 25, 50, 100, and 200 nM plotted as nanometer shift with time. *B*, same sensorgram as (*A*) but for Nb17 titrated with $CTNa_V1.5T$–CaM. *C–E*, sensorgrams showing no binding of Nb17 to CaM alone, $CTNa_V1.7T$–CaM, or $CTNa_V1.9T$, respectively. BLI, biolayer interferometry; CaM, calmodulin; Nb, nanobody; T, truncated.

(TN buffer). Beads were washed in a gravity flow column using 40 ml of TN buffer (pH 8.0) with 10 mM imidazole, and Nbs were eluted using 40 ml of TN buffer (pH 8.0) with 300 mM imidazole. Purification fractions were loaded on an any kilodalton gel and bands analyzed by SDS-PAGE, and the Nb-containing elution fractions were pooled, dialyzed at 4 °C into low-salt TN buffer (20 mM Tris–HCl, 50 mM NaCl, 2 mM DTT, pH 7.5), and concentrated to 1 mg/ml before loading on a Superdex 75 column using TN buffer. The peak fractions from gel filtration containing the Nbs were then concentrated using a 3.5 kDa cutoff filtering units to a final concentration of ∼10 to 11 mg/ml as 24 μl aliquots and flash frozen and stored at −80 °C.

Purification of CT regions of $Na_V1.4$, $Na_V1.5$, $Na_V1.7$, and $Na_V1.9$ in complex with CaM ($CTNa_V1.X$–CaM)

CT regions of $Na_V1.4$(UniProtKb:P35499), $Na_V1.5$ (UniProtKb:Q14524), $Na_V1.7$ (UniProtKb:Q15858), and $Na_V1.9$ (UniProtKb:Q9UI33) in complex with CaM (UniProtKb:P0DP23) ($CTNa_V1.X$–CaM) were used. The constructs of the CT regions of the voltage-gated sodium channel isoforms were named consistently as "truncated (T)" for constructs ending at equivalent residue of $Na_V1.4_{1764}$ and "FL" for constructs ending at equivalent residue of $Na_V1.4_{1836}$. The constructs are $CTNa_V1.4T$ with amino acids 1599 to 1764, $CTNa_V1.4FL$ with amino acids 1599 to 1836, $CTNa_V1.5T$ with amino acids 1775 to 1940, $CTNa_V1.5FL$ with amino acids 1775 to 2016, $CTNa_V1.7T$ with amino acids 1761 to 1928, $CTNa_V1.7FL$ with amino acids 1761 to 1988, $CTNa_V1.9T$ with mino acids 1605 to 1768, and $CTNa_V1.9FL$ with amino acids 1605 to 1791 (Table S1 and Fig. 3*B*). Each construct was coexpressed with mammalian CaM and purified from BL21-CodonPlus RIL cells using a GST-sepharose column followed by anion exchange chromatography and a final gel filtration chromatography step as described by Yoder *et al.* (29) with minor modifications. In brief, cells were grown overnight at 37 °C in 100 ml of LB medium supplemented with 50 μg/ml kanamycin, 20 μg/ml chloramphenicol, and 100 μg/ml carbenicillin. About 10 ml of the overnight culture was used to inoculate 1 l of LB media containing the same antibiotics. The cells were grown at 37 °C to an absorbance of 0.8 to 0.9 at 600 nm, and protein expression was induced with 1 mM IPTG.

Table 2
Kinetic and binding parameters determined by BLI for $CTNa_V1.4T$–CaM and $CTNa_V1.5T$–CaM titrated with Nb17 and Nb82

Nb (ligand)	Na_V proteins (analyte)	K_D (nM)	k_{on} (M^{-1} s^{-1})	k_{dis} (1/s)
Nb17	$CTNa_V1.4T$–CaM	41.1 ± 9.89	$1.80E^{04} \pm 3.50E^{02}$	$7.39E^{-04} \pm 1.05E^{-05}$
	$CTNa_V1.5T$–CaM	60.5 ± 5.80	$1.78E^{04} \pm 1.51E^{02}$	$1.07E^{-03} \pm 4.74E^{-06}$
Nb82	$CTNa_V1.4T$–CaM	50.2 ± 8.87	$8.98E^{03} \pm 1.32E^{02}$	$4.51E^{-04} \pm 4.41E^{-06}$
	$CTNa_V1.5T$–CaM	63.2 ± 6.75	$1.78E^{04} \pm 1.71E^{02}$	$1.13E^{-03} \pm 5.28E^{-06}$

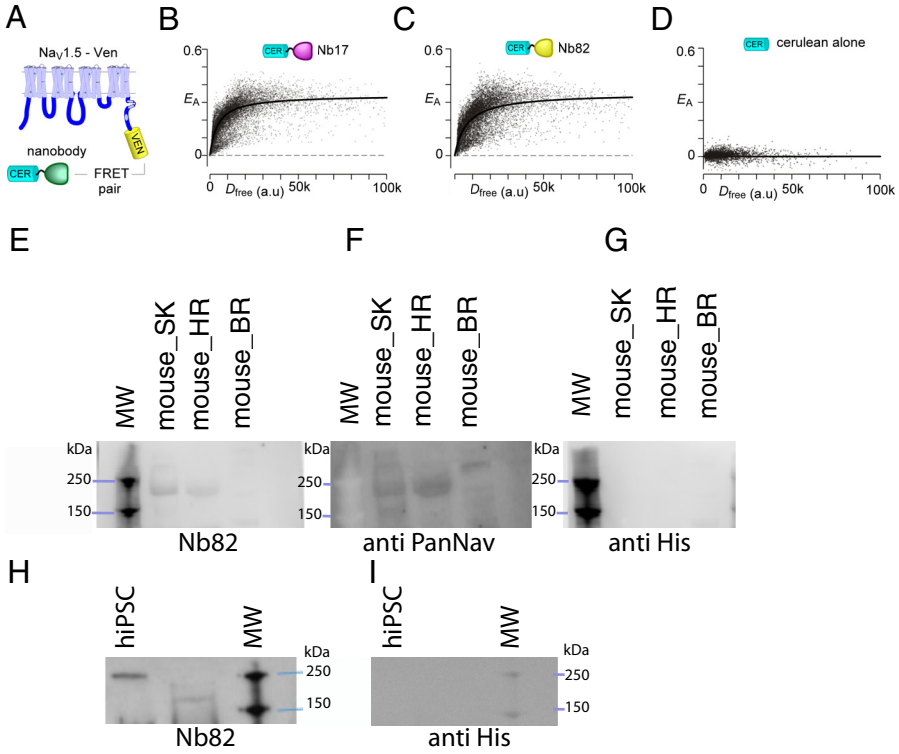

Figure 9. Nanobodies (Nbs) as tools to detect Na_V channels from live cells and tissue homogenates. *A*, schematic of FRET two-hybrid assay to probe live-cell binding of Nbs to holo-$Na_V1.5$ channels. Nbs tethered to Cerulean serve as a FRET donor, whereas Venus attached to $Na_V1.5$ serves as a FRET acceptor. *B*, robust FRET is observed between Nb17 and $Na_V1.5$. FRET efficiency (E_A) is plotted against the free donor concentration (D_{free}). Each cell represents data from a single cell. *C*, analysis of Nb82 also shows strong FRET with $Na_V1.5$. *D*, no appreciable FRET is observed between $Na_V1.5$-Venus and Cerulean alone. *E*, Western blot showing Nb82-His used as the primary antibody recognizing $Na_V1.4$(5) channels from tissues; mouse skeletal muscle, mouse heart, and brain. Blot developed using an anti-His-HRP antibody. *F*, same as (*E*) developed using the Pan-Na_V antibody (Sigma). *G*, same as (*E*) and (*F*) developed using only anti-His HRP antibody as a control. *H*, Western blot showing Nb82-His used as the primary antibody recognizing Nav1.5 from hiPSC–CMs. *I*, same as (*H*) developed using anti-His HRP antibody as a control. CM, cardiomyocyte; hiPSC, human-induced pluripotent stem cell; HRP, horseradish peroxidase.

The cells were grown overnight at 18 °C (approximately 18 h), centrifuged, and the cell pellet was frozen at −80 °C. After thawing, pellets were resuspended with PBS at 5× volume/weight ml/g of cells. DNAse was added, the cells were lysed using a microfluidizer, and the lysate was clarified at 27,500*g*. The supernatant was loaded on to a 3 ml GST resin using gravity flow. The column was washed with 30 ml wash buffer (PBS added with 100 mM NaCl), and free CaM was purified from this fraction for other experiments. The $CTNa_VT$–CaM and $CTNa_VFL$–CaM complexes were eluted in aliquots of 5 ml with an elution buffer containing 10 mM reduced L-glutathione in 50 mM Tris–HCl (pH 8.0). Eluted fractions containing protein were pooled, and 5 μg of PreScission protease was added per milligram of $CTNa_V$–CaM for cleaving the GST tag. Dialysis was performed against 2 l of buffer containing 20 mM Tris, 50 mM NaCl, 1 mM DTT, and pH 7.4. The buffer was changed twice, and the final dialysis was allowed to proceed overnight at 4 °C. The dialyzed and PreScission protease-cleaved protein was loaded on a 15 ml Source Q anion exchange column (GE). Elution was performed using buffer 20 mM Tris, 1 mM DTT, pH 7.4 and a gradient of 50 to 500 mM NaCl. Free and cleaved GST eluted at ∼8 mS/cm, and $CTNa_V$–CaM complexes eluted at between 14 and 27 mS/cm conductance that varied depending on the Na_V isoform. Fractions were judged to be >95% pure by SDS-PAGE gel and then pooled and concentrated to ∼15 to 20 mg/ml and flash frozen and stored at −80 °C. In the case of $CTNa_V1.9T$ and $CTNa_V1.9FL$, CaM did not coelute with the $CTNa_V$s unlike the other cases.

Detection of Nb specificity for Na_Vs by ELISA

Purified Nbs were assessed for recognition of Na_V proteins in high-binding 96-well plates. The analytes, purified $CTNa_VT$–CaM and $CTNa_VFL$–CaM protein isoforms ($CTNa_V1.4T$–CaM, $CTNa_V1.4FL$–CaM, $CTNa_V1.5T$–CaM, $CTNa_V1.5FL$–CaM, $CTNa_V1.7T$–CaM, and $CTNa_V1.7FL$–CaM), $CTNa_V1.9T$, $CTNa_V1.9FL$, and CaM, were diluted in PBS and coated (1 μg/well) to a 96-well plate using carbonate–bicarbonate buffer, pH 9.5, at 4 °C overnight. Next, the plate was washed five times using 100 μl/well wash buffer (PBS added with 0.1% Tween-20). Then, protein-coated wells were incubated with 100 μl/well of 0.01 μg of Nb17 or Nb82 diluted in 1× blocking buffer (PBS added with 2% BSA) for 2 h at RT on a shaking platform. The plates were then washed five times using 100 μl/well of wash buffer and incubated with mouse anti-His-peroxidase Ab at 100 mU/ml in blocking buffer for 1 h at RT. The plates were finally washed in wash buffer five times, and peroxidase activity was assayed using 100 μl/well

o-phenyl diamine in 150 mM citrate phosphate buffer and 30% H_2O_2. The plates were incubated in the dark for a few minutes until a yellow color developed in at least one of the wells. The reaction was stopped by the addition of 100 µl/well of 2 N H_2SO_4, and the absorbance was read at 450 nm (20 flashes) using a microplate reader.

DSC experiments

DSC experiments were performed using a MicroCal capillary DSC instrument. Purified Nbs, Nb17 and Nb82, were dialyzed into buffer containing 10 mM PBS, pH 8.0, with 1 mM Tris(2-carboxyethyl)phosphine, and further diluted with the dialysate to an experimental concentration of ∼0.15 mg/ml. The exact concentration of each protein solution was determined from the absorbance at 280 nm. Each solution was thoroughly degassed before loading of the calorimetric cell to have an effective volume of 138 µl. The reference cell was loaded with the dialysate. Thermal scans were conducted from 10 to 90 °C at a rate of 1 °C/min. The raw data were collected and processed using the software provided with the instrument. Data were analyzed after baselines were subtracted as described by Freire (40). The resulting transition excess heat capacity curves were fitted by nonlinear least squares in terms of reversible or irreversible denaturation models depending on whether the transitions were reversible or irreversible (33). For reversible transitions, the fitting procedure yields the calorimetric enthalpy, van't Hoff enthalpy, and transition temperature. For irreversible transitions, the fitting procedure yields the calorimetric enthalpy, activation energy, and transition temperature.

Crystallization of Nb82

Purified Nb82 was used at 10 mg/ml for all crystallization experiments. Sparse matrix commercial crystallization screens were used to find conditions in hanging-drop vapor diffusion by mixing equal volumes of Nb82 and reservoir solution. Nb82 crystallized in 2% (w/v) PEG monomethyl ether 550, 1.8 M ammonium sulfate, 0.1 M Bis–Tris, pH 6.5 was used for X-ray diffraction experiments. Crystals appeared as needles after 1 day of equilibration at 20 °C and reached 100 µm in their longest dimension on day 30. These needles were used to macro seed into 2 µl hanging-drop vapor diffusion plates with drops containing equal volumes of 10 mg/ml Nb82 and reservoir conditions optimized around the original crystallization condition varying the concentrations of PEG and ammonium sulfate. New crystals appeared in 2% (w/v) PEG monomethyl ether 550, 1.5 to 1.8 M ammonium sulfate, 0.1 M Bis–Tris, pH 6.5, on day 5. The crystals grew into cubes with largest samples being 125 µm in their longest dimension and were harvested on day 30 postseeding from the mother liquor mixed with 1 M lithium sulfate as the cryoprotectant into Hampton loops and plunge-frozen into liquid nitrogen.

Data collection and structure refinement

X-ray diffraction data of the Nb82 crystal were collected at 100 K at the NSLS II 17-ID-1 (AMX) on a DECTRIS Eiger 9M. Data were processed with fastdp (41) and XDS (42) and scaled (42) using XSCALE. Initial phases were obtained by molecular replacement using an Nb structure as search model (PDB ID: 5LMJ (14)) with the CCP4 program PHASER (43). Initial models were improved with multiple rounds of rebuilding using Coot (44) and refinement using REFMAC, version 5.8 (45). The quality of the model was assessed with Coot (44) validation tools and the wwPDB validation servers (46). Statistics are shown in Table 1. The final model contains four Nb82 molecules in the asymmetric unit.

Nb-mediated shift of Na_Vs by SEC

Mobility in-gel filtration chromatography was performed to verify formation of $CTNa_V$–CaM + Nb complexes using purified proteins (Figs. 5 and 6). Nbs and Na_Vs were mixed in a 1.2:1 M ratio, incubated for 2 h to overnight at 4 °C, and run on a Superdex 75 column using 20 mM Tris, 50 mM NaCl, and pH 7.4. Chromatograms were exported as Excel files to GraphPad Prism (GraphPad Software, Inc) for analysis and plotting. About 0.5 mg of egg-white lysozyme (14 kDa) and 0.5 mg of BSA (66 kDa) were run to serve as molecular weight gel filtration standards using the same experimental conditions to evaluate the molecular weight of the peak elution fractions.

Nb17 and Nb82 binding kinetics using BLI

Nb17 and Nb82 binding to $CTNa_V1.4$ and $CTNa_V1.5$ was measured by BLI. Data were acquired using the Data acquisition software, version 11.0, and analyzed using the Data analysis software, version 11.0 (ForteBio, Sartorius Corp). The assay was performed in kinetics mode using 200 µl protein/well in a 96-well plate format. His-tagged proteins, Nb17 and Nb82, or just buffer was immobilized on Ni–NTA biosensors. Nb17 and Nb82 loading was done at 2.5 µg/ml concentration for 300 s to prevent overcrowding and self-association of the ligand. $CTNa_V1.4T$–CaM, $CTNa_V1.5T$–CaM, $CTNa_V1.7T$–CaM, and $CTNa_V1.9T$–CaM were tested as analytes. To measure Nb association with Na_V proteins, the Nb-loaded Ni–NTA sensors were first transferred to wells containing blocking reagent (0.1% biocytin) in assay buffer for 150 s to prevent nonspecific binding and then to wells containing assay buffer until a stable baseline was reached (100 s). Following this, sensors were dipped into wells with 1:2 serially diluted Na_V proteins (at 200, 100, 50, 25, 12.5, and 6.25 nM concentrations) for 300 s followed by a 300 s dissociation step in assay buffer. All experiments were carried out at 25 °C and acquisition standard kinetics at 5 Hz with the assay plate shaking at 1000 rpm.

Flow cytometric FRET two-hybrid assay

Flow cytometric FRET two-hybrid assay for detecting Nb interaction with $Na_V1.5$ was performed as in previous studies (34). Briefly, HEK293 cells were cultured in 12-well plates and transfected with PEI 25 kDa linear polymer (Polysciences; catalog no.: 2396602). For each experiment, we cotransfected: 0.5 µg of Nb17 or Nb82 fused to Cerulean; 2 µg of Venus-tagged FL $Na_V1.5$; and 0.5 µg of t-Antigen. To test the interaction of $Na_V1.x$ isoforms to the Nbs, we cotransfected 0.5 µg

of Nb17 or Nb82 fused to Cerulean, 2 μg of Venus-tagged $CTNa_V1.x$; and 0.5 μg of t-Antigen. The cDNA pairs were mixed together in 200 μl of serum-free Dulbecco's modified Eagle's medium (DMEM) media, and 5 μl of PEI was added into each sterile tube. Following 15 min of incubation, PEI–cDNA mixtures were added to the 12-well plates, and cells were cultured for 2 days prior to experimentation. Protein synthesis inhibitor, cycloheximide (100 μM), was added to cells 2 h prior to experimentation to enhance fluorophore maturation. For FRET measurements, we utilized an LSR II (BD Biosciences) flow cytometer equipped with 405, 488, and 633 nm lasers for excitation and 18 different emission channels as previously described (34). Forward and side scatter signals were detected and used to gate for single and healthy cells. Fluorescence emission from three different channels (BV421, FITC, and BV510) were used to estimate fluorescence emission in the donor, acceptor, and FRET channels. Data were analyzed using custom MATLAB software (Mathworks).

Western blots using Nb82 to detect purified $CTNa_V$–CaM proteins

Western blot analysis was performed to assess whether Nb82 can detect $CTNa_V1.4$ and $CTNa_V1.5$ proteins using Nb82 as the primary Ab. For this, ∼1 μg/lane of purified $CTNa_V1.4T$–CaM, $CTNa_V1.4FL$–CaM, $CTNa_V1.5T$–CaM, $CTNa_V1.5FL$–CaM, $CTNa_V1.7T$–CaM, $CTNa_V1.7FL$–CaM, $CTNa_V1.9T$, $CTNa_V1.9FL$, CaM, Nb82-His, Nb17-His proteins were run on an Any kD Mini-PROTEAN TGX gel at 180 V for 30 min. Proteins were transferred using the P3 program (20 V for 10 min) of the iBlot2 protein transfer system and blocked with blocking buffer (1× PBS with Tween-20 [PBST], pH 7.4 with 5% nonfat dry milk) for 27 °C for 1 h and then washed five times in PBST (0.1% Tween-20). Proteins were incubated with Nb82-His (1 μg/ml) in blocking buffer shaking in the cold room overnight. Blots were further washed five times in PBST and probed using an anti-His-HRP-Ab at 1:500 dilutions in blocking buffer by incubating at 27 °C for 1 h with shaking. Western blot was developed and visualized using the GeneSys image acquisition software to obtain exposures at 20 s, 2 min, and 5 min. The blots were exported as tiff images and viewed and edited using ImageStudioLite (Li-COR Biosciences).

hiPSC differentiation

HiPSCs were reprogrammed from peripheral blood mononuclear cells of a healthy donor and differentiated into ventricular-like CMs by temporal modulation of Wnt signaling. Cells were cultured in basal media (RPMI1640 with 2.5 mM glutamine Gibco; catalog no.: 11875093) with B27[−] supplement without insulin (Gibco; catalog no.: 10889038) and treated with small-molecule CHIR99021 (Tocris, R&D Systems; catalog no.: 4423) on differentiation day 0 (dd0) and IWR-1 (Sigma; catalog no.: I0161) on dd3. hiPSC–CMs were replated and switched to B27(+) supplement with insulin (Gibco; catalog no.: 17504044) once they began beating ∼dd9. hiPSC–CMs were purified with lactate media from dd16 to dd20 (basal media DMEM without glucose or pyruvate [Gibco; catalog no.: 11966025]; 50 mM Hepes buffer; 100× GlutaMAX [Gibco; catalog no.: 35050061]; 100× minimum essential medium nonessential amino acids [Gibco; catalog no.: 11140050); and 4 mM sodium L-lactate [Sigma; catalog no.: L7022]). hiPSC–CMs formed an autorhythmic contracting sheet of cells and were pelleted in cold PBS on dd36 for analysis by Western blot.

Western blots using Nb82 to detect endogenous $Na_V1.4$ and $Na_V1.5$

Western blot analysis was performed to assess whether Nb82 could detect $Na_V1.4$ in skeletal muscle homogenates and Nav1.5 in heart of adult mouse and also Nav1.5 in cell lysate from hiPSC–CM. Heart muscle, brain, and quadriceps femoris muscle were collected from a 16-week-old female C57BL/6 mouse and snap frozen before analysis by Western blot. Tissue samples were crushed using a tissue-grinder pestle and resuspended in 1× PBS (pH 7.4) with 500 mM NaCl and protease inhibitors and sonicated in the cold room with a 10 s pulse–20 s pause program for a total of 10 min. Following sonication, 2% (v/v) Triton X-100 was added to the lysate and incubated on ice for 30 min. The lysate was then centrifuged in a table-top centrifuge at 10,000*g* at 4 °C for 30 min. The supernatants were mixed with equal volumes of 2× SDS-loading buffer and loaded at 40 μl/lane and run on an NuPAGE 4 to 12% Bis–Tris gel using 1× MES–SDS running buffer (Novagen) at 230 V for 72 min. Proteins were transferred, and blot was developed as described previously using blocking buffer (1× PBST [pH 7.4] with BSA). The blots were probed with Nb82 followed by anti-His-HRP detection or by pan-Na_V Ab and antimouse IgG-HRP or using anti-His-HRP Ab alone as control.

Materials and reagents

$CTNa_V$–CaM proteins

Genes coding for CT region of human Na_V ($CTNa_V$) isoforms, namely, $CTNa_V1.4T$ (amino acids 1599 to 1764), $CTNa_V1.4FL$ (amino acids 1599 to 1836), $CTNa_V1.5T$ (amino acids 1775 to 1940), $CTNa_V1.5FL$ (amino acids 1775 to 2016), $CTNa_V1.7T$ (amino acids 1761 to 1928), $CTNa_V1.7FL$ (amino acids 1761 to 1988), $CTNa_V1.9T$ (amino acids 1605 to 1768), and $CTNa_V1.9FL$ (amino acids 1605 to 1791), were subcloned into pGEX 6p1 expression vector (GenScript) and coexpressed with mammalian CaM in BL21-CodonPlus RIL *E. coli* cells (Agilent), purified using GST-sepharose 4b resin (GE Lifesciences), ReSource Q anion exchange column (GE, MilliporeSigma).

Llama immunization and Nb phage library

Freund's adjuvant (Sigma), ELISA of immune sera using MaxiSorp plates (Thermo Scientific), PBL cells isolated using Ficoll–Paque (GE Healthcare), total RNA isolation using RNeasy Midi Kit (Qiagen), restriction enzymes for cDNA amplification, PstI and NotI (New England Biolabs), *E. coli* TG1 cells (Lucigen) for phage display library, plasmid DNA isolation using QIAprep Spin Miniprep kit (QIAGEN), trypsin

(Gibco), panning in deep-well plates (Greiner Bio-One), phage ELISA primary Ab anti-HA high affinity, Roche and secondary Ab antirat IgG peroxidase-conjugate (Sigma), BSA (Sigma), BstEII (New England Biolabs). Genes coding for Nb17 and Nb82 were subcloned into pHEN6-TEV-His vector (GenScript), and Nb82 was also subcloned into pHEN6-TEV-His-StreptagII vector (GenScript); *E. coli* Rosetta-gami 2 (DE3) cells (Novagen).

Nb purification

His-Pur Ni–NTA superflow agarose (Thermo Scientific), Superdex 75 (10/300) gel filtration column (MilliporeSigma, Sigma–Aldrich), any-kDa gel 10-15well (Mini-PROTEAN TGX Precast gel; Bio-Rad) 3.5 kDa cutoff concentrators (polyethersulfone membrane; MilliporeSigma).

Protein ELISAs and Western blots

About 96-well EIA/RIA plates (Costar-9018), anti-His-peroxidase secondary Ab (Roche), Tecan infinite M1000 microplate reader (Tecan i-control; 2.0.10.0 application), iBlot2 transfer stack (Thermo Scientific; catalog no.: IB24001), iBlot2 protein transfer system (Thermo Scientific), anti-His-HRP-Ab (Sigma; catalog no.: 11965085001), pan-Na_V Ab (Sigma; catalog no.: S8809), 1 μg/ml of antimouse IgG-HRP-Ab (Cell Signaling; catalog no.: 7076S), and Supersignal West Pico chemiluminescent substrate (Thermo Fisher Scientific; catalog no.: 34080).

Cell culture

HEK293 cells (American Type Culture Collection; catalog no.: CRL-1573), DMEM with 4.5 g/l D-glucose, 110 mg/l sodium pyruvate, 2 mM L-glutamine (Gibco; catalog no.: 11995040), additional 4 mM L-glutamine (Gibco; catalog no.: 35650061), fetal bovine serum (Sigma; catalog no.: F2442), and PEI 25 kDa linear polymer (Polysciences; catalog no.: 2396602). Human $Na_V1.5$ construct corresponds to clone M77235.1 (GenBank). Reagents and small molecules for hiPSC culture and differentiation: basal media (RPMI 1640 with 2.5 mM glutamine; Gibco; catalog no.: 11875093), B27(–) supplement without insulin (Gibco; catalog no.: 10889038), CHIR99021 (Tocris, R&D Systems; catalog no.: 4423), IWR-1 (Sigma; catalog no.: I0161), and B27(+) supplement with insulin (Gibco; catalog no.: 17504044). Lactate purification media: (basal media DMEM without glucose or pyruvate (Gibco; catalog no.: 11966025); 50 mM Hepes buffer; 100× GlutaMAX (Gibco; catalog no.: 35050061); 100× minimum essential medium nonessential amino acids (Gibco; catalog no.: 11140050); 4 mM sodium L-lactate (Sigma; catalog no.: L7022).

CTNaV1.x constructs for flow cytometric FRET two-hybrid assay

Venus coding sequence followed to the coding sequence for a triple alanine and FL $Na_V1.5$ was cloned in pcDNA3.1. The Venus-AAA-$CTNa_V1.x$ contains the coding sequence for $CTNa_V1.1$ (amino acids 1788 to 2009), $CTNa_V1.2$ (amino acids 1775 to 2005), $CTNa_V1.3$ (amino acids 1770 to 2000), $CTNa_V1.4$ (amino acids 1598 to 1835), $CTNa_V1.5$ (amino acids 1771 to 2016), $CTNa_V1.6$ (amino acids 1765 to 1980), $CTNa_V1.7$ (amino acids 1759 to 1988), $CTNa_V1.8$ (amino acids 1721 to 1956), and $CTNa_V1.9$ (amino acids 1603 to 1791).

Equipment/apparatus

Octet RED96e instrument (ForteBio, Sartorius Corp), MicroCal capillary cell Differential Scanning Calorimeter (Malvern Panalytical), Akta purification system, SLA1500 rotor (Thermo Fisher Scientific), microfluidizer (Microfluidics Corporation), Q125 sonicator (QSonica), Mosquito for 96-well plate screens (SPT Labtech), NSLS II 17-ID-1 beamline equipped with a DECTRIS Eiger 9M detector, LSR II Flow cytometer for FRET two-hybrid assay (BD Biosciences).

Data availability

The structure presented in this article has been deposited in the PDB with PDB ID: 7R63. All clones and constructs will be shared upon request to gabelli@jhmi.edu. All remaining data are contained within this article and the supporting information.

Supporting information—This article contains supporting information (14, 29, 30, 41–46).

Acknowledgments—We thank the technical assistance of Inmunova (Buenos Aires, Argentina) for supporting llama immunization. We thank Chulan Kwon for providing mouse tissue and David Suh for technical assistance. This work was funded by the National Institutes of Health (NIH)/National Heart, Lung, and Blood Institute (grant no.: HL128743). We thank Dr Robert Cole for help with mass spectrometry analysis carried out at the Johns Hopkins University School of Medicine Mass Spectrometry and Proteomics Facility, which is supported by the Sidney Kimmel Comprehensive Cancer Center (National Cancer Institute/NIH grant: 2P30 CA006973) and Hopkins Conte NIH/National Institute of Diabetes and Digestive and Kidney Diseases Basic and Translational Research Core Center (grant no.: P30 DK089502). Work at the AMX (17-ID-1) and FMX (17-ID-2) beamlines was supported by National Institute of General Medical Sciences, NIH (grant no.: P41GM111244) and by the US Department of Energy Office of Biological and Environmental Research grant (grant no.: KP1605010), and the National Synchrotron Light Source II at Brookhaven National Laboratory is supported by the Department of Energy Office of Basic Energy Sciences under contract number DE-SC0012704 (grant no.: KC0401040). Flow cytometry was performed in the CCTI Flow Cytometry Core, supported in part by the Office of the Director, NIH under awards S10RR027050. We acknowledge the use of the Eukaryotic Tissue Culture Facility at the Johns Hopkins University and the guidance of its manager, Dr Yana Li.

Author contributions—L. M. A. and S. B. G. conceptualization; L. S., V. A., and M. B.-J. methodology; L. S., V. A., and M. B.-J. validation; L. S., V. A., and A. S. formal analysis; L. S., V. A., D. S., S. N., A. S., and M. B.-J. investigation; V. A., D. S., S. N., J. B. Y., K. M. W., S. K., J. N. N., F. A. G., A. S., E. F., G. F. T., and M. B.-J. resources; S. B. G. data curation; L. S., L. M. A., and S. B. G. writing–original draft; L. S., V. A., D. S., S. N., J. B. Y., K. M. W., S. K., J. N. N., M. S. L., F. A. G., A. S., E. F., G. F. T., L. M. A., M. B.-J., and S. B. G. writing–reviewing & editing; L. S. visualization; G. F. T., L. M. A., and S. B. G.

supervision; S. B. G. project administration; G. F. T., L. M. A., M. B.-J., and S. B. G. funding acquisition.

Funding and additional information—J. N. N. was supported by the NIH grant (grant no.: R25 GM109441) and the Vivien Thomas Scholars Initiative at Johns Hopkins University. The content is solely the responsibility of the authors and does not necessarily represent the official views of the NIH.

Conflict of interest—S. B. G. is a founder and holds equity in Advanced Molecular Sciences LLC. S. B. G. is consultant to Genesis Therapeutics and Xinthera, Inc. All other authors declare that they have no conflicts of interest with the contents of this article.

Abbreviations—The abbreviations used are: Ab, antibody; BLI, biolayer interferometry; BSA, bovine serum albumin; CaM, calmodulin; cDNA, complementary DNA; CDR3, complementarity-determining region 3; CM, cardiomyocyte; CT, C-terminal region; dd, differentiation day; DMEM, Dulbecco's modified Eagle's medium; DSC, differential scanning calorimetry; FL, full length; GST, glutathione-S-transferase; HA, hemagglutinin; HEK293, human embryonic kidney 293 cell line; hiPSC, human-induced pluripotent stem cell; HRP, horseradish peroxidase; Na_V, voltage-gated sodium channel; Nb, nanobody; Ni, nickel; NIH, National Institutes of Health; NTA, nickel–nitrilotriacetic acid; PBL, peripheral blood lymphocyte; PBST, PBS with Tween-20; PDB, Protein Data Bank; RT, room temperature; SEC, size-exclusion chromatography; T, truncated; TES, Tris–HCl, EDTA, and sucrose buffer; TN, Tris and NaCl buffer; VHH, variable domain of heavy chain of heavy-chain antibody.

References

1. Fozzard, H. A., and Hanck, D. A. (1996) Structure and function of voltage-dependent sodium channels: Comparison of brain II and cardiac isoforms. *Physiol. Rev.* **76**, 887–926
2. George, A. L., Jr. (2005) Inherited disorders of voltage-gated sodium channels. *J. Clin. Invest.* **115**, 1990–1999
3. Escayg, A., MacDonald, B. T., Meisler, M. H., Baulac, S., Huberfeld, G., An-Gourfinkel, I., Brice, A., LeGuern, E., Moulard, B., Chaigne, D., Buresi, C., and Malafosse, A. (2000) Mutations of SCN1A, encoding a neuronal sodium channel, in two families with GEFS+2. *Nat. Genet.* **24**, 343–345
4. Wallace, R. H., Scheffer, I. E., Barnett, S., Richards, M., Dibbens, L., Desai, R. R., Lerman-Sagie, T., Lev, D., Mazarib, A., Brand, N., Ben-Zeev, B., Goikhman, I., Singh, R., Kremmidiotis, G., Gardner, A., *et al.* (2001) Neuronal sodium-channel alpha1-subunit mutations in generalized epilepsy with febrile seizures plus. *Am. J. Hum. Genet.* **68**, 859–865
5. Wulff, H., Christophersen, P., Colussi, P., Chandy, K. G., and Yarov-Yarovoy, V. (2019) Antibodies and venom peptides: New modalities for ion channels. *Nat. Rev. Drug Discov.* **18**, 339–357
6. Hutchings, C. J., Colussi, P., and Clark, T. G. (2019) Ion channels as therapeutic antibody targets. *MAbs* **11**, 265–296
7. Che, T., English, J., Krumm, B. E., Kim, K., Pardon, E., Olsen, R. H. J., Wang, S., Zhang, S., Diberto, J. F., Sciaky, N., Carroll, F. I., Steyaert, J., Wacker, D., and Roth, B. L. (2020) Nanobody-enabled monitoring of kappa opioid receptor states. *Nat. Commun.* **11**, 1145
8. van der Linden, R. H., Frenken, L. G., de Geus, B., Harmsen, M. M., Ruuls, R. C., Stok, W., de Ron, L., Wilson, S., Davis, P., and Verrips, C. T. (1999) Comparison of physical chemical properties of llama VHH antibody fragments and mouse monoclonal antibodies. *Biochim. Biophys. Acta* **1431**, 37–46
9. De Genst, E., Silence, K., Decanniere, K., Conrath, K., Loris, R., Kinne, J., Muyldermans, S., and Wyns, L. (2006) Molecular basis for the preferential cleft recognition by dromedary heavy-chain antibodies. *Proc. Natl. Acad. Sci. U. S. A.* **103**, 4586–4591
10. Stortelers, C., Pinto-Espinoza, C., Van Hoorick, D., and Koch-Nolte, F. (2018) Modulating ion channel function with antibodies and nanobodies. *Curr. Opin. Immunol.* **52**, 18–26
11. Williams, W. A., Linley, J. E., Jones, C. A., Shibata, Y., Snijder, A., Button, J., Hatcher, J. P., Huang, L., Taddese, B., Thornton, P., Schofield, D. J., Thom, G., Popovic, B., Dosanjh, B., Wilkinson, T., *et al.* (2019) Antibodies binding the head domain of P2X4 inhibit channel function and reverse neuropathic pain. *Pain* **160**, 1989–2003
12. Danquah, W., Meyer-Schwesinger, C., Rissiek, B., and Koch-Nolte, F. (2016) Nanobodies that block gating of the P2X7 ion channel ameliorate inflammation. *Sci. translational Med.* **8**, 366ra162
13. Garza, J. A., Taylor, A. B., Sherwood, L. J., Hart, P. J., and Hayhurst, A. (2017) Unveiling a drift resistant cryptotope within marburgvirus nucleoprotein recognized by llama single-domain antibodies. *Front. Immunol.* **8**, 1234
14. Duhoo, Y., Roche, J., Trinh, T. T. N., Desmyter, A., Gaubert, A., Kellenberger, C., Cambillau, C., Roussel, A., and Leone, P. (2017) Camelid nanobodies used as crystallization chaperones for different constructs of PorM, a component of the type IX secretion system from Porphyromonas gingivalis. *Acta Crystallogr. F Struct. Biol. Commun.* **73**, 286–293
15. Herce, H. D., Deng, W., Helma, J., Leonhardt, H., and Cardoso, M. C. (2013) Visualization and targeted disruption of protein interactions in living cells. *Nat. Commun.* **4**, 2660
16. Ries, J., Kaplan, C., Platonova, E., Eghlidi, H., and Ewers, H. (2012) A simple, versatile method for GFP-based super-resolution microscopy *via* nanobodies. *Nat. Methods* **9**, 582–584
17. Buser, D. P., Schleicher, K. D., Prescianotto-Baschong, C., and Spiess, M. (2018) A versatile nanobody-based toolkit to analyze retrograde transport from the cell surface. *Proc. Natl. Acad. Sci. U. S. A.* **115**, E6227–E6236
18. Senders, M. L., Hernot, S., Carlucci, G., van de Voort, J. C., Fay, F., Calcagno, C., Tang, J., Alaarg, A., Zhao, Y., Ishino, S., Palmisano, A., Boeykens, G., Meerwaldt, A. E., Sanchez-Gaytan, B. L., Baxter, S., *et al.* (2019) Nanobody-facilitated multiparametric PET/MRI phenotyping of atherosclerosis. *JACC Cardiovasc. Imaging* **12**, 2015–2026
19. Wang, L., Zhang, L., Huang, B., Li, K., Hou, G., Zhao, Q., Wu, C., Nan, Y., Du, T., Mu, Y., Lan, J., Chen, H., and Zhou, E. M. (2019) A nanobody targeting viral nonstructural protein 9 inhibits porcine reproductive and respiratory syndrome virus replication. *J. Virol.* **93**, e01888-18
20. Yu, C., Wang, L., Rowe, R. G., Han, A., Ji, W., McMahon, C., Baier, A. S., Huang, Y. C., Marion, W., Pearson, D. S., Kruse, A. C., Daley, G. Q., Wu, H., and Sliz, P. (2020) A nanobody targeting the LIN28:let-7 interaction fragment of TUT4 blocks uridylation of let-7. *Proc. Natl. Acad. Sci. U. S. A.* **117**, 4653–4663
21. Caussinus, E., Kanca, O., and Affolter, M. (2011) Fluorescent fusion protein knockout mediated by anti-GFP nanobody. *Nat. Struct. Mol. Biol.* **19**, 117–121
22. Ruoff, K., Kilic, T., Devant, J., Koromyslova, A., Ringel, A., Hempelmann, A., Geiss, C., Graf, J., Haas, M., Roggenbach, I., and Hansman, G. (2019) Structural basis of nanobodies targeting the prototype norovirus. *J. Virol.* **93**, e02005-18
23. De Haard, H. J., Bezemer, S., Ledeboer, A. M., Muller, W. H., Boender, P. J., Moineau, S., Coppelmans, M. C., Verkleij, A. J., Frenken, L. G., and Verrips, C. T. (2005) Llama antibodies against a lactococcal protein located at the tip of the phage tail prevent phage infection. *J. Bacteriol.* **187**, 4531–4541
24. Duarte, J. N., Cragnolini, J. J., Swee, L. K., Bilate, A. M., Bader, J., Ingram, J. R., Rashidfarrokhi, A., Fang, T., Schiepers, A., Hanke, L., and Ploegh, H. L. (2016) Generation of immunity against pathogens *via* single-domain antibody-antigen constructs. *J. Immunol.* **197**, 4838–4847
25. Scully, M., Cataland, S. R., Peyvandi, F., Coppo, P., Knobl, P., Kremer Hovinga, J. A., Metjian, A., de la Rubia, J., Pavenski, K., Callewaert, F., Biswas, D., De Winter, H., Zeldin, R. K., and Investigators, H. (2019) Caplacizumab treatment for acquired thrombotic thrombocytopenic purpura. *N. Engl. J. Med.* **380**, 335–346
26. Detalle, L., Stohr, T., Palomo, C., Piedra, P. A., Gilbert, B. E., Mas, V., Millar, A., Power, U. F., Stortelers, C., Allosery, K., Melero, J. A., and

Depla, E. (2016) Generation and characterization of ALX-0171, a potent novel therapeutic nanobody for the treatment of respiratory syncytial virus infection. *Antimicrob. Agents Chemother.* **60**, 6–13
27. Shilo, M., Motiei, M., Hana, P., and Popovtzer, R. (2014) Transport of nanoparticles through the blood-brain barrier for imaging and therapeutic applications. *Nanoscale* **6**, 2146–2152
28. Gabelli, S. B., Boto, A., Kuhns, V. H., Bianchet, M. A., Farinelli, F., Aripirala, S., Yoder, J., Jakoncic, J., Tomaselli, G. F., and Amzel, L. M. (2014) Regulation of the $Na_V1.5$ cytoplasmic domain by calmodulin. *Nat. Commun.* **5**, 5126
29. Yoder, J. B., Ben-Johny, M., Farinelli, F., Srinivasan, L., Shoemaker, S. R., Tomaselli, G. F., Gabelli, S. B., and Amzel, L. M. (2019) Ca(2+)-dependent regulation of sodium channels $Na_V1.4$ and $Na_V1.5$ is controlled by the post-IQ motif. *Nat. Commun.* **10**, 1514
30. Pardon, E., Laeremans, T., Triest, S., Rasmussen, S. G., Wohlkonig, A., Ruf, A., Muyldermans, S., Hol, W. G., Kobilka, B. K., and Steyaert, J. (2014) A general protocol for the generation of Nanobodies for structural biology. *Nat. Protoc.* **9**, 674–693
31. Nguyen, V. S., Logger, L., Spinelli, S., Desmyter, A., Le, T. T., Kellenberger, C., Douzi, B., Durand, E., Roussel, A., Cascales, E., and Cambillau, C. (2015) Inhibition of type VI secretion by an anti-TssM llama nanobody. *PLoS One* **10**, e0122187
32. Wang, Y., Li, R., Qiao, S., Wang, J., Liu, H., Li, Z., Ma, H., Yang, L., Ruan, H., Weng, M., Hiscox, J. A., Stewart, J. P., Nan, Y., Zhang, G., and Zhou, E. M. (2020) Structural characterization of non-structural protein 9 complexed with specific nanobody pinpoints two important residues involved in porcine reproductive and respiratory syndrome virus replication. *Front. Microbiol.* **11**, 581856
33. Schon, A., and Freire, E. (2021) Reversibility and irreversibility in the temperature denaturation of monoclonal antibodies. *Anal. Biochem.* **626**, 114240
34. Rivas, S., Hanif, K., Chakouri, N., and Ben-Johny, M. (2021) Probing ion channel macromolecular interactions using fluorescence resonance energy transfer. *Methods Enzymol.* **653**, 319–347
35. Robertson, A. D., and Murphy, K. P. (1997) Protein structure and the energetics of protein stability. *Chem. Rev.* **97**, 1251–1268
36. Schon, A., Clarkson, B. R., Jaime, M., and Freire, E. (2017) Temperature stability of proteins: Analysis of irreversible denaturation using isothermal calorimetry. *Proteins* **85**, 2009–2016
37. Morgenstern, T. J., Park, J., Fan, Q. R., and Colecraft, H. M. (2019) A potent voltage-gated calcium channel inhibitor engineered from a nanobody targeted to auxiliary CaVbeta subunits. *eLife* **8**, e49253
38. Alzogaray, V., Urrutia, M., Berguer, P., Rossi, A., Zylberman, V., Pardo, R., Bonomi, H. R., and Goldbaum, F. A. (2019) Characterization of folding-sensitive nanobodies as tools to study the expression and quality of protein particle immunogens. *J. Biotechnol.* **293**, 17–23
39. Madeira, F., Park, Y. M., Lee, J., Buso, N., Gur, T., Madhusoodanan, N., Basutkar, P., Tivey, A. R. N., Potter, S. C., Finn, R. D., and Lopez, R. (2019) The EMBL-EBI search and sequence analysis tools APIs in 2019. *Nucleic Acids Res.* **47**, W636–W641
40. Freire, E. (1995) Differential scanning calorimetry. *Methods Mol. Biol.* **40**, 191–218
41. Winter, G., and McAuley, K. E. (2011) Automated data collection for macromolecular crystallography. *Methods* **55**, 81–93
42. Kabsch, W. (2010) Xds: Integration, scaling, space-group assigment and post refinement. *Acta Crystallogr. D Biol. Crystallogr.* **66**, 125–132
43. McCoy, A. J., Grosse-Kunstleve, R. W., Adams, P. D., Winn, M. D., Storoni, L. C., and Read, R. J. (2007) Phaser crystallographic software. *J. Appl. Crystallogr.* **40**, 658–674
44. Emsley, P., Lohkamp, B., Scott, W. G., and Cowtan, K. (2010) Features and development of Coot. *Acta Crystallogr. D Biol. Crystallogr.* **66**, 486–501
45. Collaborative Computational Project, N. (1994) The CCP4 suite: Programs for protein crystallography. *Acta Crystallogr. D Biol. Crystallogr.* **50**, 760–763
46. Berman, H., Henrick, K., and Nakamura, H. (2003) Announcing the worldwide protein Data Bank. *Nat. Struct. Biol.* **10**, 980